nature communications

Article

https://doi.org/10.1038/s41467-025-65636-9

# Piezo1-mediated mechanotransduction controls osteocyte maturation and dendrite development via a YAP-CCN-Src signaling axis

Received: 23 September 2024

Accepted: 20 October 2025

Published online: 28 November 2025

Check for updates

Yizhong Jenny Hu, Xinchen Wu, Fuhua Wang, Yu Jin, Yangchen Jin, Yuchen Liu, Qian Cong & Yingzi Yang

Mechanical force controls bone development and homeostasis, with mechanosensitive osteocytes playing a key role. Osteocytes form interconnected dendrites to respond to mechanical stimuli and regulate bone formation and resorption. However, the molecular mechanisms underlying osteocyte maturation and dendrite formation remain elusive. Here we show that Piezo1 loss in late osteoblasts and osteocytes reduces bone mass and disrupts osteocyte differentiation with reduced dendrite number, length and network formation. Decreased YAP activity and unexpected Wnt/β-catenin signaling activation cause these deficiencies, largely restored by intermittent YAP activation. We further identify YAP targets CCN1/2 as crucial secreted factors in the Piezo1-YAP mechanotransduction. CCN1/2 overexpression in the liver rescues dendritic and bone defects in the Piezo1 mutant mice by activating Src, promoting actin polymerization, and activating YAP in a positive feedforward loop. Our findings highlight the pivotal roles of Piezo1 and YAP-CCN1/2-Src signaling, offering potential therapeutic targets for improving osteocyte dendritic networks.

Mechanical force is a fundamental regulator of both embryonic development and postnatal homeostasis[1,2]. Sensing and responding to mechanical stimuli at the molecular, cellular and tissue level are critical for organisms to adapt to the changing environment and thrive. Mechanotransduction is particularly important in the bone, which is a major load-bearing component of the body that supports and protects internal organs as well as enables movements[3,4]. Local loading shapes bone structure and morphology and plays a crucial role in regulating bone strength. Increased loading results in bone gain, while prolonged bed rest or exposure to anti-gravity leads to bone loss[5,6]. Therefore, it is imperative to understand the cellular and molecular regulation of mechanotransduction in bone biology and disorders. Bone homeostasis involves the coordination of the bone-forming osteoblasts and bone-resorbing osteoclasts, both are regulated by osteocytes, the most abundant and mechanosensitive cell type in the bone[7]. Osteocytes are differentiated from osteoblasts and reside in the fluid-filled lacunae of the canalicular system, anchored to the surrounding pericellular and extracellular matrix by tethering fibers[8]. Deeply embedded in the bone tissue, osteocytes are equipped with long and interconnected dendrites that form a network to sense and propagate mechanical stimuli such as matrix strain, and fluid flow in the perilacunar space that induces shear stress. These mechanical stimuli activate a variety of mechanosensors in the osteocyte cell bodies or dendrites, such as gap junction, integrin, primary cilium, and ion channels[9]. Recently, the stretch-activated cation channel Piezo1 has been identified as the only one directly

Department of Developmental Biology, Harvard School of Dental Medicine; Harvard Stem Cell Institute, Boston, MA, USA.
e-mail: yingzi_yang@hsdm.harvard.edu

https://doi.org/10.1038/s41467-025-65636-9

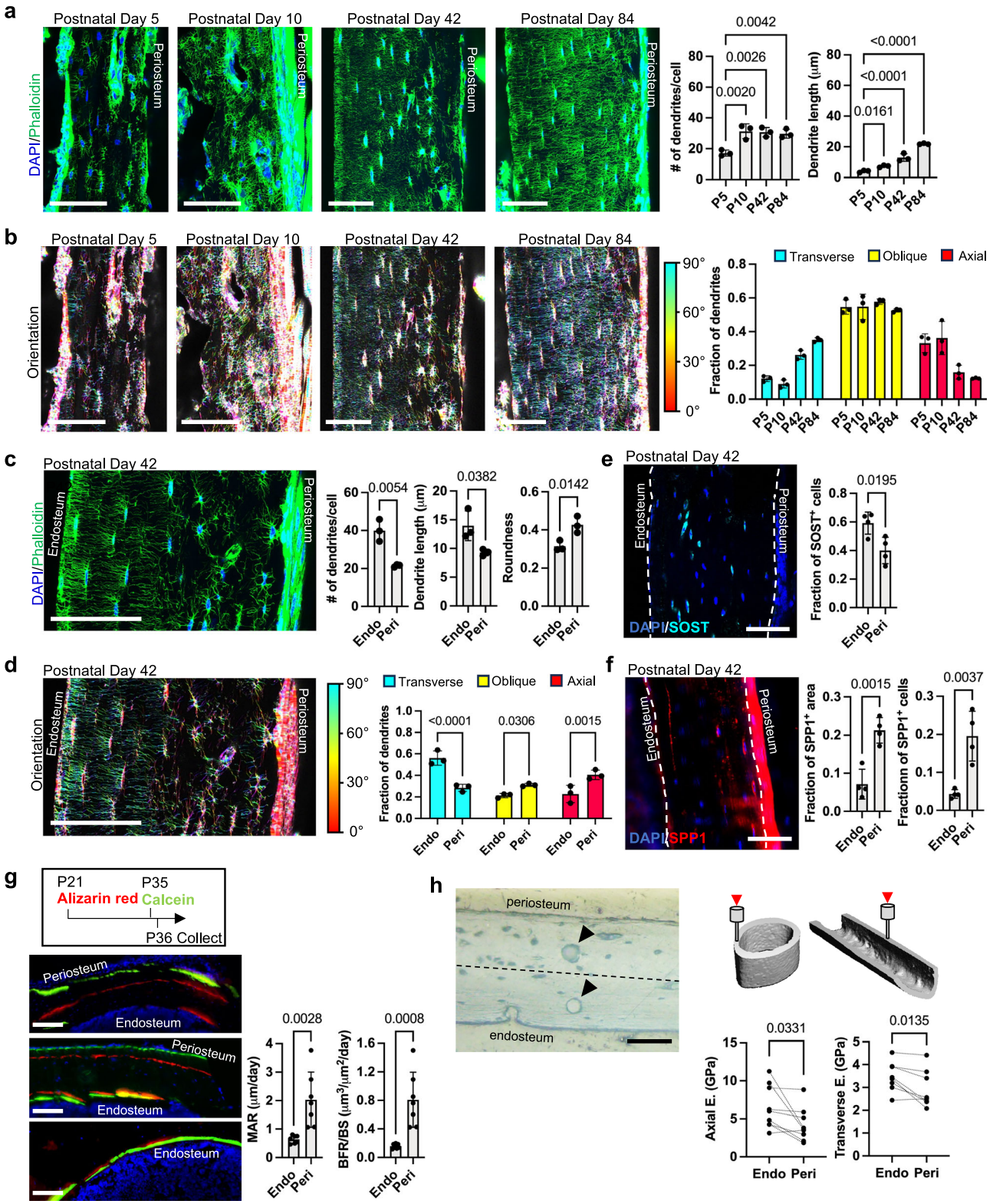


gated by force and critically regulates skeletal development and homeostasis[10–13].

Osteocytes regulate osteoblasts and osteoclasts via secreted factors such as sclerostin (SOST), receptor activator of nuclear factor kappa-B ligand (RANKL), and osteoprotegerin[14]. Osteocytes also directly remodel the surrounding matrix in response to mechanical stress by regulating matrix metalloproteases expression[15]. Osteocytes undergo drastic morphological changes, such as elongation and shrinkage of the cell body, formation and growth of the dendritic processes, as well as alteration of gene expression, when they mature from osteoblasts. While osteocytes upregulate the expression of dentin matrix acidic phosphoprotein (*Dmp1*), *Sost*, phosphate regulating endopeptidase X-linked (*Phex*), fibroblast growth factor 23 (*Fgf23*) and RANKL (*Tnfsf11*)[16,17], they also express lower levels of osteoblast-enriched genes such as secreted phosphoprotein 1 (*Spp1*), type I collagen, alpha 1 (*Col1A1*) and Sp7 transcription factor (*Sp7*). Relative to the cell body, osteocyte dendrites are more responsive to mechanical stimuli in vitro in an integrin β3-dependent manner[18–20].

**Fig. 1 | Osteocyte maturation is associated with bone matrix stiffening.** **a** Phalloidin staining (green; nucleus: blue) and osteocyte dendrite quantification of WT femur midshaft cortical bone at the indicated ages. $N = 3$ biological replicates. **b** Analysis and quantification of osteocyte dendrite orientation. Color bar indicates fiber angle with respect to the long bone axis. Axial (red): 0–30°, Oblique (yellow): 30–60°, Transverse (cyan): 60–90°. $N = 3$ biological replicates. **c** Phalloidin (green; nucleus: blue) staining and osteocyte dendrite quantification on the endosteal (endo) and periosteal (peri) side of WT femur midshaft cortical bone at postnatal day 42. $N = 3$ biological replicates. **d** Analysis and quantification of osteocyte dendrite orientation (Axial: red; Oblique: yellow; Transverse: cyan) at postnatal day 42. $N = 3$ biological replicates. **e** IF staining and quantification of SOST expression (cyan; nucleus: blue) in WT femur midshaft cortical bone at postnatal day 42. $N = 4$ biological replicates. **f** IF staining of SPP1 expression (red; nucleus: blue) at postnatal day 42. $N = 4$ biological replicates. **g** Dynamic histomorphometry analysis of femur midshaft cortical bone. Alizarin red (red) and calcein (green) were injected at the indicated time points. Nucleus is stained blue. MAR mineral apposition rate. BFR/BS bone formation rate per bone surface. $N = 7$ biological replicates. **h** Schematic of microindentation on WT femur midshaft cortical bone tissue at postnatal day 42. Triangles indicate imprints made from paired indentations on the periosteal and endosteal sides. E elastic modulus. $N = 8$ (transverse) and 9 (axial) paired indentations. Scale bars: **a**–**j** 50 μm. Bar graphs represent mean ± SD. **a** One-way ANOVA with Bonferroni's post-hoc correction. **c**–**g** Two-sided unpaired Student's *t* test. **h** Two-sided paired Student's t-test. Source data are provided as a Source Data file.

Dendritic glycocalyx is shown to promote integrin attachment and hemichannel opening, critical for signal transduction in response to mechanical loading[18]. Dendrites from neighboring osteocytes interconnect to form the dendritic network via gap junctions[18,21]. The strikingly dense dendritic network is believed to imbue osteocytes tremendous mechanotransduction capability for maintaining normal bone mass, which disconnects and deteriorates in aged and osteoporotic bone, suggesting the critical roles of the dendritic processes in regulating bone homeostasis[22–24]. Furthermore, unloading by sciatic nerve resection resulted in blunted osteocyte dendrite development[25], suggesting a critical role for mechanical stimuli to maintain osteocyte dendritic structures. However, despite the key functions of osteocyte dendrites, the mechanisms underlying osteocyte maturation and dendrite formation remain elusive.

Several recent studies have identified potential pathways regulating dendrite formation and osteocyte maturation[26–29], as well as osteocyte perilacunar remodeling, which was also linked to reduced bone mechanical property[30,31]. Importantly, osteoblast/osteocyte-specific deletion of transcriptional co-activators YAP and TAZ, which are critical transcriptional mediators of mechanotransduction, results in impaired bone mass and reduced dendritic network[32,33].

In this study, we reveal the essential role of Piezo1-mediated mechanotransduction in driving the cellular and molecular changes of osteocytes via control of YAP and Wnt/β-catenin signaling. We further uncover a molecular signaling axis mediated by CCN1/2 downstream of YAP in driving osteocyte dendrite formation. We demonstrate that osteocyte dendrite morphology and network are robustly controlled by YAP and its downstream signaling effectors, uncovering potential therapeutic targets in combating loading/unloading-induced bone loss.

## Results

### Progressive maturation of osteocytes during postnatal bone development

To study osteocyte maturation, we stained F-actin, the major cytoskeletal component within osteocyte dendrites[34]. During postnatal development, dendrite number and length increased continuously (Fig. 1a), gradually forming a highly ordered network in adult bone (Fig. 1b). Cell density and size reduced over time, with increased elongation of cell body (Supplementary Fig. 1a). To investigate whether this morphological maturation correlates to gene expression changes, we analyzed a bulk RNA sequencing (RNAseq) dataset of mouse long bones[35] (Supplementary Fig. 1b). Expression of osteocyte markers *Sost* and *Fgf23* increased with age, while expression of osteoblast markers *Spp1*, *Alpl*, *Sp7*, and *Col1A1* decreased. These results suggest a progressive cellular and molecular maturation of osteocytes during postnatal bone development.

### Osteocytes on the periosteal to endosteal sides show distinct morphologies in postnatal bone development

In young adults, we observed progressive changes in osteocyte morphology from the periosteum to the endosteum (Fig. 1c, d). Periosteal osteocytes resembled those from an earlier stage (Fig. 1a), more rounded with fewer, shorter, and less aligned dendrites. Immunofluorescent (IF) staining detected more $SOST^+$ cells on the endosteal side (Fig. 1e), while SPP1 expression was higher in periosteal osteoblasts and osteocytes (Fig. 1f). These results suggest that osteocyte maturation is spatially asymmetric and immature osteocytes are observed mostly on the periosteum side.

While both the endosteum and periosteum harbor skeletal progenitors, appositional bone growth primarily occurs at the periosteal front[36–38]. To directly assess bone apposition, we performed dynamic histomorphometry in young mice. At P21, alizarin red labeled continuously mineralizing surfaces on the periosteal side (Supplementary Fig. 1c). Quantification of mineral apposition rate and bone formation rate (BFR) indicated more net bone formation on the periosteal surface (Fig. 1g). Osteoclasts localized to the endosteum (Supplementary Fig. 1d), consistent with previous findings[39]. Therefore, prior to skeletal maturation, new bone formation, which contains newly embedded osteocytes, was more active on the periosteal surface than on the endosteal surface. These data may explain the gradual maturation we observed from the periosteal to endosteal surface in midshaft cortical bone.

### Osteocyte maturation is associated with bone matrix stiffening

Bone formation begins with collagen matrix synthesis, followed by gradual mineral accumulation that confers mechanical strength[40], reflected in increased tissue mineral density (TMD) over time (Supplementary Fig. 1e). To assess whether osteocyte maturation is associated with tissue mechanical properties, we performed microindentation on paired sites from the periosteal and endosteal fraction (Fig. 1h). Higher axial and transverse elastic moduli, indicating a stiffer bone matrix, were detected on the endosteal side. These results suggest that both osteocyte maturation and bone matrix stiffening progress more frequently from the periosteal to the endosteal side, which aligns with earlier research demonstrating the regulation of osteocyte dendrite formation and elongation by mechanical stimuli[25,41,42].

### Piezo1 is required for osteocyte maturation and dendrite formation

We therefore investigated whether Piezo1, a force-gated ion channel, regulates osteocyte maturation and dendrite formation. Using *Dmp1Cre*, *Piezo1* was removed in late osteoblasts and osteocytes (Supplementary Fig. 2a)[43,44]. *Dmp1Cre; Piezo1$^{f/f}$* (*Piezo1* cKO) mice showed significant cortical and trabecular bone loss and increased osteoclast number compared to *Piezo1$^{f/f}$* (wild type, WT) mice (Supplementary Fig. 2b, c), consistent with prior studies[10,12]. *Piezo1* loss did not change osteocyte density or size but reduced osteoblast proliferation and increased cell death (Supplementary Fig. 2d–f). We detected reductions in dendrite number and length in the *Piezo1* cKO mice (Fig. 2a), as well as increased cell roundness (Supplementary Fig. 2e). Dendrites in mutant mice displayed reduced transverse fibers and increased axial fibers, reminiscent of immature osteocytes

https://doi.org/10.1038/s41467-025-65636-9

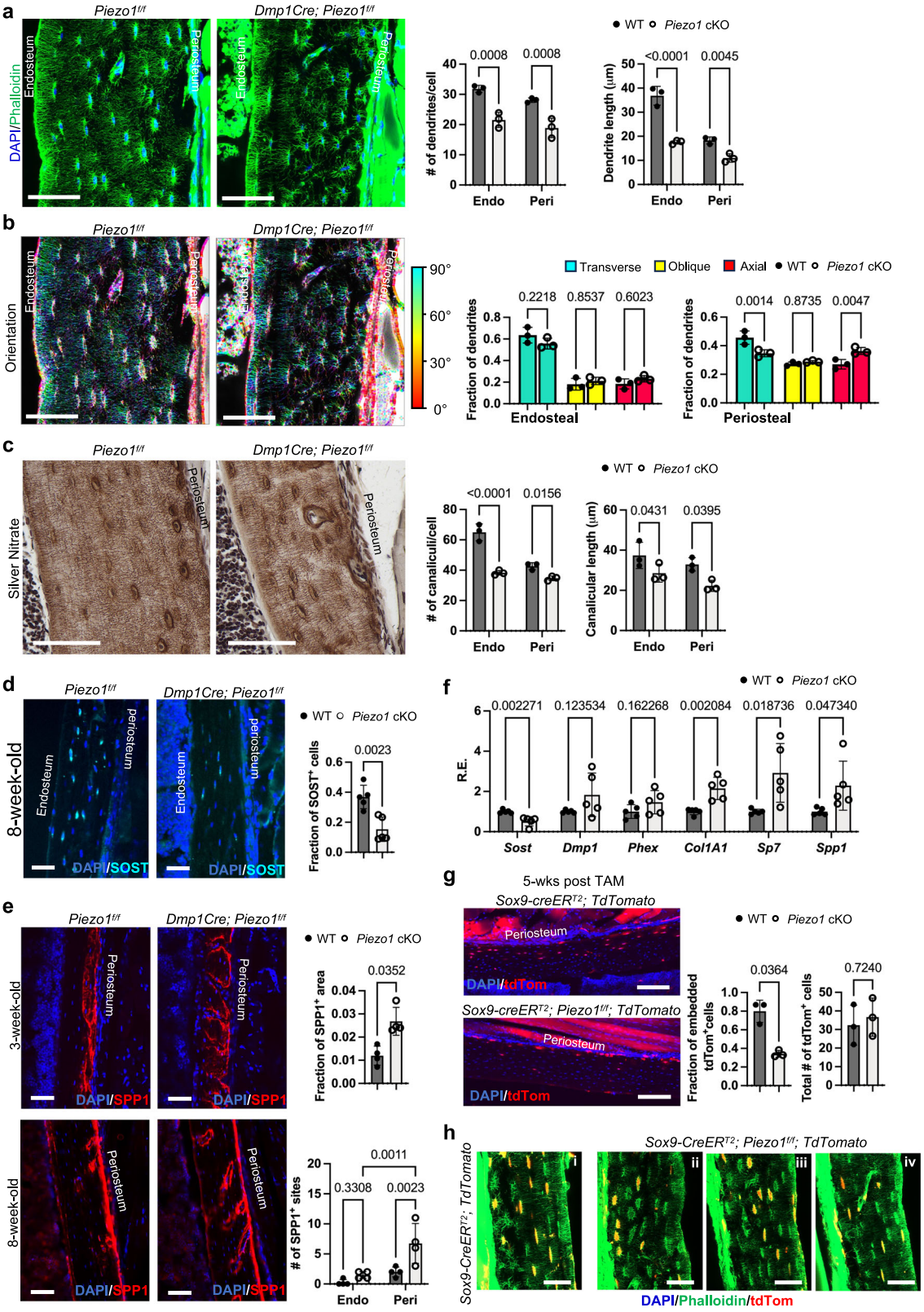


(Fig. 2b). Analysis of the lacunar canalicular network (LCN), critical for bone mechanoresponse[45], detected reduced canalicular number and length (Fig. 2c). Younger *Piezo1* cKO mice showed impaired development of dendritic network at each stage, indicating that *Piezo1* loss delays the progressive maturation of osteocyte dendrites (Supplementary Fig. 2g). Similar reductions in osteocyte number and length due to *Piezo1* loss was also found in trabecular bone osteocytes (Supplementary Fig. 2h).

In the *Piezo1* cKO mouse bones, we detected reduced protein levels of SOST, DMP1, and PHEX (Fig. 2d, Supplementary Fig. 2i, j), while SPP1 was increased within the bone matrix of the *Piezo1* cKO mice, forming discrete clusters containing embedded osteocytes that

**Fig. 2 | Piezo1 is required for osteocyte maturation and dendrite formation.** **a** Phalloidin staining (green; nucleus: blue) and osteocyte dendrite quantification of femur midshaft cortical bone in 8-week-old WT and *Dmp1Cre; Piezo1$^{f/f}$* (*Piezo1* cKO) mice. $N = 3$ biological replicates. **b** Analysis and quantification of osteocyte dendrite orientation in 8-week-old WT and *Piezo1* cKO mice. Color bar indicates the fiber angle with respect to the long bone axis. Axial (red): 0°–30°. Oblique (yellow): 30–60°. Transverse (cyan): 60–90°. $N = 3$ biological replicates. **c** Silver nitrate staining and quantification of LCN in 8-week-old WT and *Piezo1* cKO mice. $N = 3$ biological replicates. **d** IF staining and quantification of SOST expression (cyan; nucleus: blue) in 8-week-old WT and *Piezo1* cKO mice. $N = 5$ biological replicates. **e** IF staining and quantification of SPP1 expressions (red; nucleus: blue) in 8-week-old WT and *Piezo1* cKO mice. $N = 4$ biological replicates. **f** QRT-PCR analysis of mRNA expressions of osteocyte (*Sost*, *Dmp1*, *Phex*) and osteoblast genes (*Col1A1*, *Sp7*, *Spp1*) in cortical bone tissue of 8-week-old WT and *Piezo1* cKO mice. $N = 5$ biological replicates. **g** Analysis of embedding osteocytes (red) in femur midshaft cortical bone from *Sox9-CreER$^{T2}$; TdTomato* and *Sox9-CreER$^{T2}$; Piezo1$^{f/f}$; TdTomato* mice. Red: tdTomato. Blue: nucleus. TAM was injected at P21. Mice were collected 5-weeks post-TAM injection. $N = 3$ biological replicates. **h** Phalloidin staining (green; tdTomato: red) of femur midshaft cortical bone from *Sox9-CreER$^{T2}$; TdTomato* and *Sox9-CreER$^{T2}$; Piezo1$^{f/f}$; TdTomato* mice, quantified in Supplementary Fig. 2k. $N = 5$ biological replicates. Scale bars: (**a**–**e**, **g**, **h**) 50 μm. Bar graphs represent mean ± SD. (**a**–**g**) Two-sided unpaired Student's *t* test. Source data are provided as a Source Data file.

were connected to the periosteal surface (Fig. 2e). At the mRNA level, *Sost* expression reduced, while *Spp1*, *Alpl*, *Sp7*, and *Col1a1* expression increased in the *Piezo1* cKO mice (Fig. 2f). We did not detect changes in *Dmp1* or *Phex* mRNA expression, possibly due to the complexity of gene expression regulation. These findings collectively suggest that Piezo1 is crucial for osteocyte differentiation.

To investigate whether Piezo1 regulates the transition from surface osteoblasts to matrix-embedded osteocytes, we generated the *Sox9-CreER$^{T2}$; Piezo1$^{f/f}$; Rosa$^{tdTomato}$* mice and compared them with the *Sox9-CreER$^{T2}$; Rosa$^{tdTomato}$* mice, which marks progenitor osteoblasts on the periosteal surface[46] (Fig. 2g). In the mutant mice, fewer tdTom$^+$ cells were embedded into the bone matrix. To investigate potential non-cell-autonomous effects, we analyzed osteocyte morphology of tdTom$^+$ mutant cells and their surrounding tdTom$^-$ cells in the *Sox9-CreER$^{T2}$; Piezo1$^{f/f}$; Rosa$^{tdTomato}$* mice (Fig. 2h, Supplementary Fig. 2k). Clusters of tdTom$^+$ cells in regions with frequent recombination were more rounded with reduced dendrite number and length compared to tdTom$^+$ cells of WT mice. TdTom$^+$ cells surrounded by WT cells had normal osteocyte morphology and dendrite number with moderate reductions in dendrite length. These findings suggest that WT cells may rescue dendritic defects in *Piezo1*-deficient cells. Piezo1's role in osteocyte maturation and dendrite development may therefore involve non-cell-autonomous mechanisms.

## Mechanosensing by Piezo1 promotes osteocyte maturation and dendrite formation

To investigate the mechanistic role of force and Piezo1 in regulating osteocyte maturation, we stimulated OCY454 cells, an osteocyte cell line[47], with different modes of mechanical stimulation. Culturing OCY454 cells in 3D collagen hydrogel at 37 °C, which supports osteocyte differentiation, promoted dendrite formation (Supplementary Fig. 3a). Matrix stiffening (MS) and fluid shear stress (FSS) increased dendrite number and length (Fig. 3a, b, Supplementary Fig. 3b–d), indicating that mechanical stimulation promotes osteocyte dendrite formation. These changes were recapitulated by treating OCY454 cells with Yoda1, a pharmacological activator of Piezo1[48]. To directly assess the requirement of Piezo1, we generated a *Piezo1* "knock-out" (KO) cell line (*Piezo1$^{-/-}$* OCY454) (Supplementary Fig. 3e). *Piezo1* KO cells exhibited reduced dendrite number and length and failed to respond to MS or FSS (Fig. 3c, d, Supplementary Fig. 3f, g). Overexpression of WT *Piezo1* in the *Piezo1* KO OCY454 cells restored dendrite formation (Supplementary Fig. 3h), further demonstrating that Piezo1 is essential for sensing mechanical stimulation to facilitate dendrite formation during osteocyte differentiation.

In addition to the morphological defects, we detected reduced expression of *Dmp1*, *Phex*, and *Sost* and increased expression of *Sp7*, Runt-related transcription factor 2 (*Runx2*), and bone gamma-carboxyglutamate protein (*Bglap*) in *Piezo1* KO OCY454 cells (Fig. 3e). Similar changes were detected at each stage of osteocyte differentiation (Supplementary Fig. 3i), indicating *Piezo1* loss impairs the transcriptional maturation to osteocytes, consistent with our in vivo findings.

## Piezo1 promotes osteocyte differentiation by activating YAP and inhibiting Wnt signaling

To identify the molecular mechanism underlying Piezo1's role in osteocyte maturation and morphogenesis, we performed transcriptional profiling of WT and *Piezo1* KO OCY454 cells during differentiation. Using differentially expressed genes (DEGs) across time points in WT cells, we identified 4 gene sets based on their dynamic changes during normal differentiation (Fig. 3f, Supplementary Data 1). We performed the Kyoto Encyclopedia of Genes and Genomes (KEGG) pathway analysis to identify unique pathways associated with each gene set (Supplementary Fig. 3j). Gene set enrichment analysis (GSEA) showed elevated Wnt/β-catenin signaling (Fig. 3g, Supplementary Fig. 3k) and reduced Hippo/YAP signaling (Fig. 3h, Supplementary Fig. 3l) in *Piezo1* KO cells. Differentiation of WT cells exhibited a progressive increase in YAP activity and decrease in Wnt/β-catenin signaling (Fig. 3i). These trends were reversed in the *Piezo1* KO cells, confirmed by quantitative real-time polymerase chain reaction (qRT-PCR) analysis of YAP target genes cysteine-rich angiogenic inducer 61 (*Cyr61*) and connective tissue growth factor (*Ctgf*)[49], as well as Wnt/β-catenin signaling target genes axis inhibition protein 2 (*Axin2*) and lymphoid enhancer-binding factor 1 (*Lef1*)[50] (Supplementary Fig. 3m).

In the *Dmp1Cre; Piezo1$^{f/f}$; Rosa$^{tdTomato}$* postnatal mouse bones, IF staining identified reduced YAP and increased β-catenin and LEF1 protein levels (Fig. 3j–l). These changes were detected in both tdTom$^+$ and tdTom$^-$ cells, suggesting cell-autonomous and non-cell-autonomous regulation. Elevated Wnt/β-catenin signaling was further confirmed by increased Axin2-GFP expression[51] in the *Piezo1* cKO mice (Fig. 3m). Additionally, we found reduced expression of *Cyr61* and increased expression of *Axin2* and *Lef1* (Fig. 3n). Collectively, these data suggest that Piezo1 may regulate osteocyte maturation and dendrite formation by activating YAP and inhibiting Wnt/ β-catenin signaling.

We then activated YAP in OCY454 cells with TDI-011536[52] and inhibited Wnt/β-catenin signaling with LGK974[53], which increased osteocyte dendrite number and length as well as *Dmp1* and *Sost* expressions (Fig. 4a–c, Supplementary Fig. 4a, b). Conversely, activating Wnt/β-catenin signaling by CHIR99021[54] or inhibiting YAP by verteporfin[55] reduced dendrite length and/or number (Fig. 4a, b). Considering the cytotoxicity of verteporfin, we also inhibited YAP by overexpressing a dominant-negative TEAD4[56], which reduced dendrite number and length without increasing cell death (Supplementary Fig. 4c). These results suggest that YAP activation and Wnt/β-catenin inhibition directly promote the cellular and molecular maturation of osteocytes.

Interestingly, treatment with a higher dose of TDI-011536 reduced dendrite length and promoted cell clustering (Supplementary Fig. 4d). Physiological mechanical stimulation is a dynamic process alternating loading and unloading conditions. Considering YAP activation downstream of Piezo1 is likely dynamic[57], we investigated whether intermittent YAP activation could enhance the effects on osteocyte dendrite formation (Supplementary Fig. 4e). Intermittent TDI-011536 treatment increased dendrite number and length while preventing cell

https://doi.org/10.1038/s41467-025-65636-9

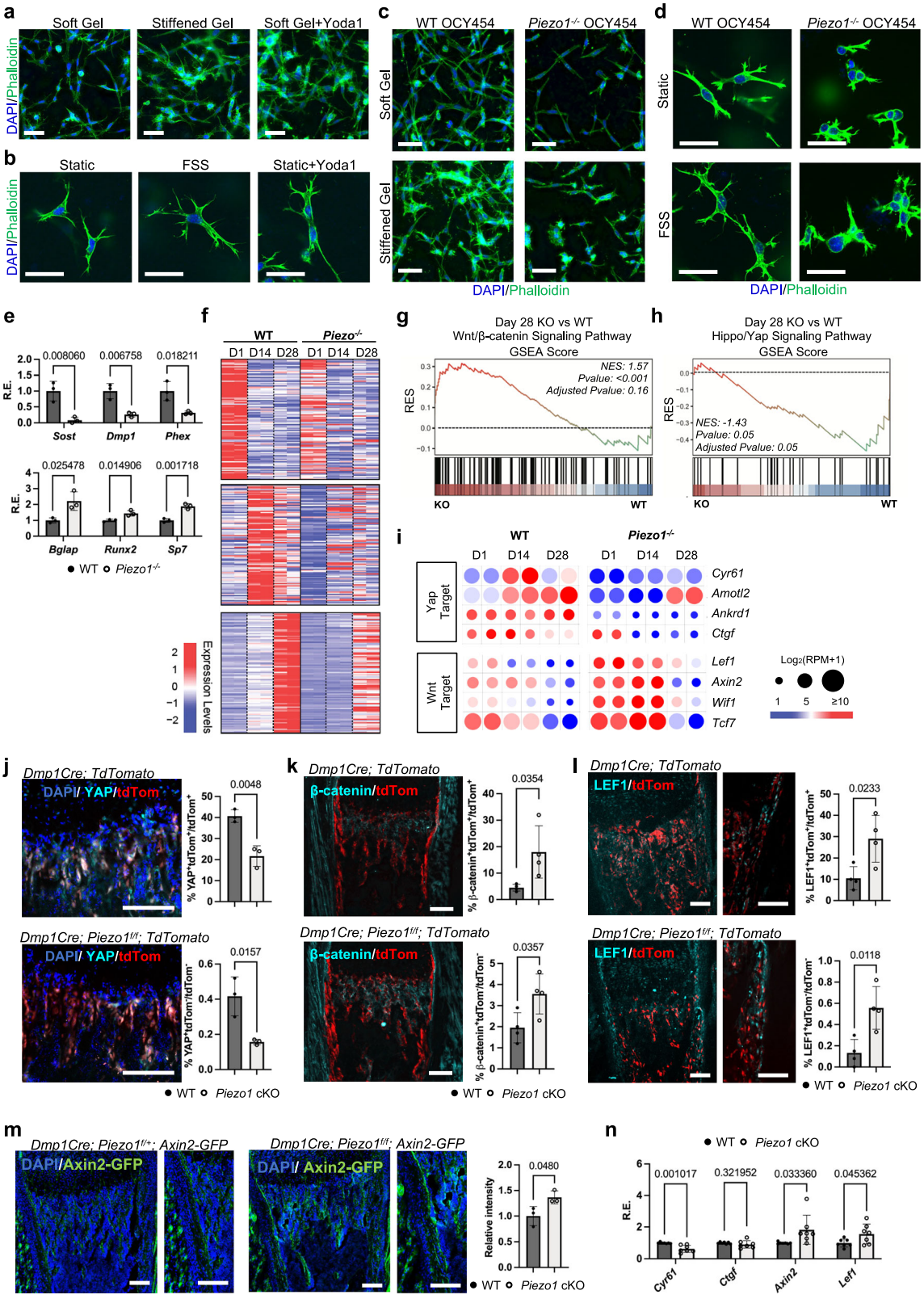


aggregation (Fig. 4d). Compared to constant TDI-011536 treatment, intermittent treatment resulted in slightly more reduction of phosphorylated-YAP (pYAP), with more robust induction of YAP target genes *Cyr61*, *Ctgf* and ajuba LIM protein (*Ajuba*)[58] (Supplementary Fig. 4f, g). Furthermore, intermittent TDI-011536 treatment increased the expression of *Dmp1*, *Sost* and *Fgf23*, while these parameters were unchanged or even reduced by constant TDI-011536 treatment (Supplementary Fig. 4h), suggesting that dynamic activation of YAP is critical for osteocyte maturation.

In the *Piezo1* KO cells, intermittent TDI-011536 and LGK974 treatments restored dendrite number and length, as well as *Dmp1* expression (Fig. 4e, f, Supplementary Fig. 4i). These findings indicate that *Piezo1* regulates osteocyte maturation through YAP activation and Wnt/β-catenin inhibition. Combined treatment with TDI-011536 and

**Fig. 3 | Piezo1 regulates osteocyte maturation by activating YAP and inhibiting Wnt signaling. a** Dendrites (green; nucleus: blue) of WT OCY454 cells in 3D collagen hydrogels with MS or 1 μM Yoda1 for 3 days, quantified in Supplementary Fig. 3c. $N = 3$ independent experiments. **b** Dendrites (green; nucleus: blue) of WT OCY454 cells with FSS or 1 μM Yoda1 for 3 days, quantified in Supplementary Fig. 3d. $N = 3$ independent experiments. **c** Dendrites (green; nucleus: blue) of WT and *Piezo1*$^{-/-}$ OCY454 cells in soft and stiffened hydrogel, quantified in Supplementary Fig. 3f. $N = 3$ independent experiments. **d** Dendrites (green; nucleus: blue) of WT and *Piezo1*$^{-/-}$ OCY454 cells under FSS, quantified in Supplementary Fig. 3g. $N = 3$ independent experiments. **e** qRT-PCR analysis of *Sost*, *Dmp1*, *Phex*, *Bglap*, *Runx2*, and *Sp7* expressions in WT and *Piezo1*$^{-/-}$ OCY454 cells after 21 days of differentiation. $N = 3$ independent experiments. **f** Bulk RNA-seq analysis of WT and *Piezo1*$^{-/-}$ OCY454 cells at the indicated time points of differentiation. Heatmap shows gene sets unique to each time point in WT cells. $N = 2$ independent experiments. **g**, **h** GSEA of Wnt/β-catenin and Hippo/YAP signaling pathways comparing *Piezo1*$^{-/-}$ to WT OCY454 cells. NES normalized enrichment score. One-sided Kolmogorov–Smirnov–like running-sum statistic with permutation testing and FDR correction for multiple comparisons. **i** YAP and Wnt target gene expression from RNA-seq analysis. **j**–**l** IF staining of YAP (cyan; nucleus: blue; tdTomato: red; $N = 3$ biological replicates), β-catenin (cyan; nucleus: blue; tdTomato: red; $N = 4$ biological replicates) and LEF1 (cyan; nucleus: blue; tdTomato: red; $N = 4$ biological replicates) in P1 WT and *Piezo1* cKO femurs. **m** Analysis of Wnt/β-catenin signaling activation using *axin2-GFP* reporter (green; nucleus: bluemice in WT and *Piezo1* cKO mice femurs at P1. $N = 3$ biological replicates. **n** YAP (*Cyr61*, *Ctgf*) and Wnt/β-catenin (*Axin2*, *Lef1*) target gene expressions in 8-week-old WT and *Piezo1* cKO mice. $N = 7$ biological replicates. Scale bar: (**a**–**d**) 100 μm, (**j**–**m**) 50 μm. Bar graphs represent mean ± SD. (**e**, **j**–**n**) Two-sided unpaired Student's *t* test. Source data are provided as a Source Data file.

LGK974 showed better rescue of osteocyte dendrite morphology (Supplementary Fig. 5a, b). Interestingly, TDI-011536 treatment robustly reduced *Lef1* and *Axin2* expressions, while LGK974 treatment moderately increased *Ctgf* and *Cyr61* expressions (Supplementary Fig. 5c). These findings suggest that YAP and Wnt/β-catenin signaling may antagonize each other during osteocyte maturation, and YAP activation may act upstream of Wnt/β-catenin signaling inhibition.

Osteocyte differentiation promoted the expression of *Sost* (Supplementary Fig. 3i), a secreted negative regulator of bone mass that inhibits Wnt/β-catenin signaling[59]. Treatment with a recombinant human SOST (rhSOST) protein promoted dendrite formation in WT cells and rescued dendrite defects in *Piezo1* KO cells (Fig. 4g, Supplementary Fig. 5d, e). Consistently, *Sost*-KO mice showed reduced dendrite and canalicular density compared to WT mice (Fig. 4h, Supplementary Fig. 5f), as well as significantly increased SPP1$^{+}$ osteoblasts within the bone matrix (Supplementary Fig. 5g). These results suggest that while *Sost* loss results in activation of osteoblasts that increase bone mass[60], SOST secretion by osteocytes may also enhance their own differentiation via a cell-autonomous mechanism.

## Intermittent YAP activation rescues dendritic and bone defects in the *Piezo1*-deficient mice

To test whether YAP activity modulates osteocyte dendrite formation in vivo, we activated YAP in *Dmp1*-expressing cells using a doxycycline (Dox)-inducible system (TetOYAP)[61]. We first compared the effects of intermittent and constant YAP activation (YAP gain) (Supplementary Fig. 6a). *Ctgf* expression was robustly induced in both YAP gain groups, while *Cyr61* expression was only induced by intermittent YAP activation (Supplementary Fig. 6b). Periosteal dendrite and canalicular density were increased in both YAP gain groups (Fig. 5a, b, Supplementary Fig. 6c, d). However, constant YAP activation reduced dendrite and canalicular length and increased cell roundness (Supplementary Fig. 6c–e).

Both YAP gain groups showed significant increases in cortical and trabecular bone mass (Fig. 5c, d). However, body weight and femur length were reduced by constant YAP activation, while preserved by intermittent YAP activation. These differential effects were further investigated. We found that constant YAP gain resulted in poor bone quality with reduced TMD and disorganized collagen fibrils (Fig. 5d, e). Dynamic histomorphometry revealed woven bone formation by constant YAP activation, while intermittent YAP activation promoted normal lamellar bone formation (Fig. 5f, Supplementary Fig. 5f). Consistent with previous findings, we found that the SPP1$^{+}$ osteoblasts and their proliferation, which were restricted to the bone surface in the WT bone, were drastically increased in the woven bone matrix by constant YAP activation, but not by intermittent YAP activation (Fig. 5g, Supplementary Fig. 6h, i). Additionally, constant YAP activation reduced expression of osteocyte markers DMP1 and PHEX, while intermittent YAP activation preserved or further increased their expression (Fig. 5h, i, Supplementary Fig. 6i, j, Supplementary Fig. 4h). Expression of MMP13, critical for osteocyte perilacunar remodeling and maintaining bone's mechanical property[30], was reduced by constant YAP activation but preserved by intermittent YAP activation (Fig. 5j, Supplementary Fig. 5k, l). Collectively, these results indicate that osteocyte differentiation and dendritic network formation during normal cortical bone formation requires dynamic YAP activation, which can result from physiological loading. Constant YAP activation impairs osteocyte differentiation, and results in pathological formation of woven bone.

We therefore intermittently activated YAP in *Piezo1* cKO mice and found that three cycles of Dox treatment improved cortical and trabecular BV/TV (Supplementary Fig. 6m, Supplementary Table 1). Strikingly, five cycles of Dox treatment completely restored cortical and trabecular bone mass (Fig. 5k, l, Supplementary Fig. 6n). Cortical and trabecular dendrite density and length, as well as LCN in *Piezo1* cKO mice were also restored to control levels (Fig. 5m, Supplementary Fig. 6o, q, r), although increased cell roundness due to *Piezo1* loss was not rescued (Supplementary Fig. 6p). Molecularly, intermittent YAP activation in the *Piezo1* cKO mice normalized *Sost* expression, reduced *Spp1* and *Sp7* expression, indicating that the osteocyte differentiation defects due to *Piezo1* loss were rescued (Supplementary Fig. 6s). Interestingly, intermittent YAP activation in the *Piezo1* cKO mice also reduced *Axin2* and *Lef1* expression, indicating that elevated Wnt signaling in response to *Piezo1* loss is at least partially due to reduced YAP activity (Supplementary Fig. 6t). These data suggest that intermittent YAP activation is sufficient to maintain dendritic structures and bone mass in osteocytes.

We next asked whether reducing the upregulated Wnt/β-catenin signaling in the *Piezo1* cKO mice in vivo could restore osteocyte dendritic defects by treating mice with low-dose LGK974[62] (Fig. 6a). Six hours after a single administration of LGK974, expression of *Dmp1* and *Phex* increased (Fig. 6b). Five weeks of LGK974 treatment increased dendrite number but not LCN in WT mice (Fig. 6c, Supplementary Fig. 7a). Defects in dendritic and LCN due to Piezo1-deficiency were partially rescued by LGK974 treatment. We did not observe differences in osteoblast/osteocyte marker expression in the *Piezo1* cKO mice after LGK974 treatment (Supplementary Fig. 7b).

Considering the systemic effects of LGK974 treatment, we partially removed β-catenin (*Ctnnb1*$^{fl/+}$) in *Dmp1*-expressing cells in WT and *Piezo1* cKO mice, which restored dendritic and LCN defects in the *Piezo1* cKO mice (Fig. 6d, Supplementary Fig. 7c). Neither LGK974 nor partial removal of *Ctnnb1* improved bone mass in WT or *Piezo1* cKO mice despite rescued dendritic structures (Fig. 6e–h), likely due to impaired osteoblast differentiation and increased osteoclastic resorption due to reduced Wnt/β-catenin signaling[11,63–65]. Collectively, these data suggest that while both YAP and Wnt/β-catenin regulate dendrite formation, YAP signaling plays a more dominant role in the regulation of bone mass.

## Piezo1 promotes dendrite formation via activation of the YAP-CCN1/2-Src signaling axis

During dendrite formation, cells undergo drastic cytoskeletal remodeling[17]. Since YAP is a key transcription regulator, we

https://doi.org/10.1038/s41467-025-65636-9

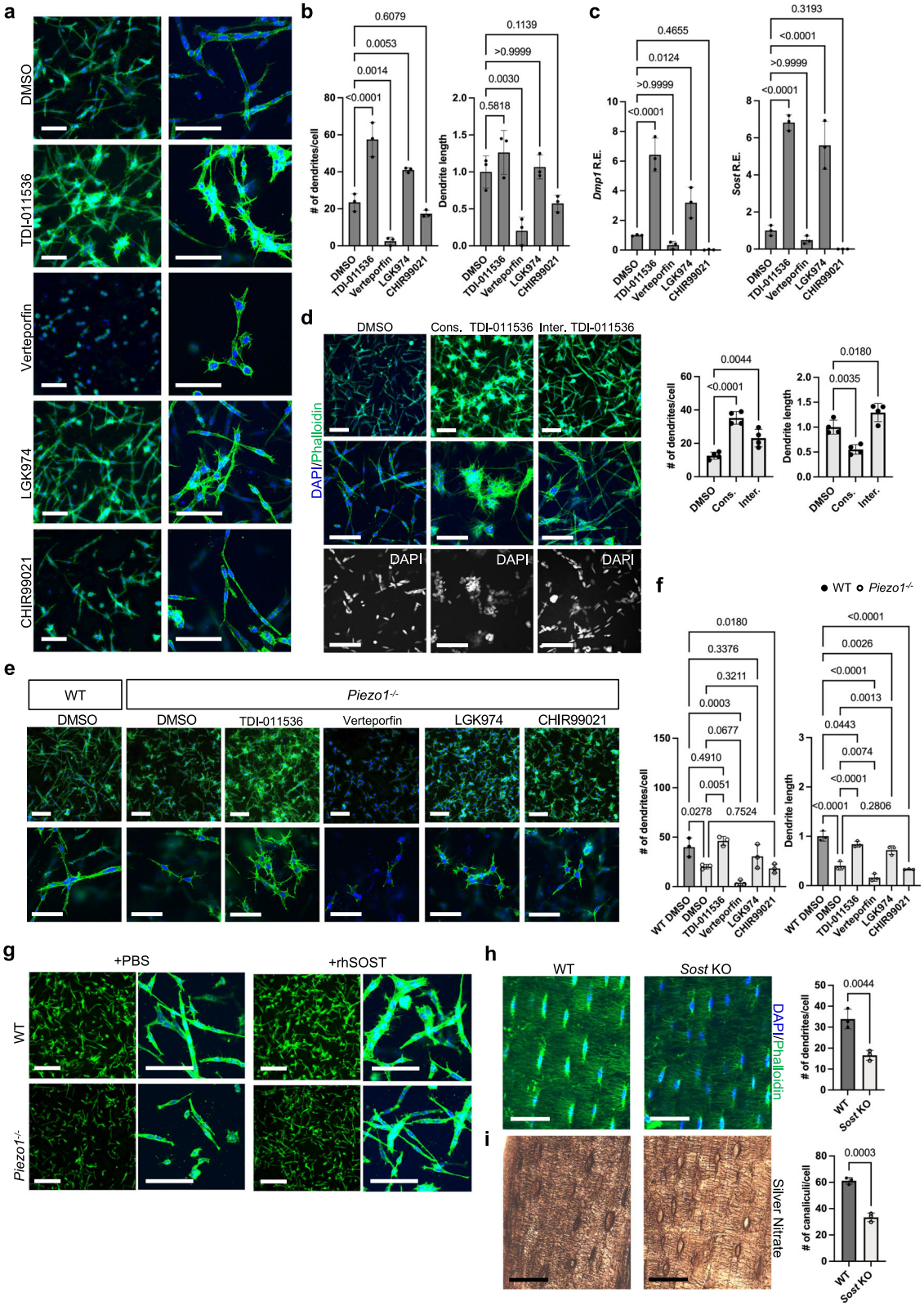


investigated YAP target genes *Cyr61* and *Ctgf*, which encode secreted proteins CCN1 and CCN2, respectively[49,66]. CCN1 and CCN2 are ECM-associated proteins that can induce actin cytoskeleton rearrangement[67]. We hypothesized that Piezo1-mediated YAP-activation may control dendrite formation by directly regulating cytoskeleton reorganization via CCN1 and CCN2.

We first tested whether CCN1 and CCN2 can promote dendrite development in vitro. We cultured OCY454 cells in the presence of Huh-7, a hepatocyte cell line[68], overexpressing GFP, CCN1, and/or CCN2 (Fig. 7a). CCN1 alone increased dendrite number and length in WT cells (Fig. 7b, Supplementary Fig. 8a). While CCN2 alone had no effect, CCN1 and CCN2 together resulted in significantly more and longer dendrites. As *Cyr61* and *Ctgf* expression was reduced in the *Piezo1* KO OCY454 cells (Supplementary Fig. 3m), we further asked whether restoring CCN1 and CCN2 can rescue the dendritic defects caused by *Piezo1* deficiency. Indeed, CCN1/2 rescued dendrite number

**Fig. 4 | YAP and Wnt/β-catenin signaling regulate osteocyte maturation in vitro. a**, **b** Phalloidin staining (green; nucleus: blue) and osteocyte dendrite quantification of WT OCY454 cells treated with 300 nM TDI-011536, 50 nM Verteporfin, 500 nM LGK974 and 500 nM CHIR99021 for 3 days. $N = 3$ independent experiments. **c** QRT-PCR analysis of mRNA expressions of *Sost* and *Dmp1* subjected to pharmacological treatments in for 2 days. $N = 3$ independent experiments. **d** Phalloidin staining (green; nucleus: blue) and osteocyte dendrite quantification of WT OCY454 cells under constant or intermittent treatment of 1 mM TDI-011536 for 3 days. $N = 4$ independent experiments. **e**, **f** Phalloidin staining (green; nucleus: blue) and osteocyte dendrite quantification of DMSO-treated WT OCY454 cells and *Piezo1*$^{-/-}$ OCY454 cells treated with DMSO, 300 nM TDI-011536, 50 nM Verteporfin, 500 nM LGK974 and 500 nM CHIR99021 for 3 days. $N = 3$ independent experiments. **g** Phalloidin staining (green; nucleus: blue) of WT and *Piezo1*$^{-/-}$ OCY454 cells treated with 100 ng/mL recombinant human SOST protein (rhSOST) for 7 days, quantified in Supplementary Fig. 5e. $N = 3$ independent experiments. **h**, **i** Phalloidin (green; nucleus: blue) and silver nitrate staining with quantification of osteocyte dendrites and LCN in femur midshaft cortical bone of 11-week-old WT and *Sost*-KO mice. $N = 3$ biological replicates. Scale bar: (**a**, **d**, **e**, **g**) 100 μm, (**h**) 20 μm. Bar graphs represent mean ± SD. (**b**–**d**, **f**) One-way ANOVA with Bonferroni's post-hoc correction. **i** Two-sided unpaired Student's *t* test. Source data are provided as a Source Data file.

and length, as well as *Dmp1* expression in the *Piezo1* KO OCY454 cells (Fig. 7c, Supplementary Fig. 8b, c).

Dendritic structures of osteocytes transduce mechanical signals[18]. To further test whether CCN1/2 signaling restores osteocyte mechanotransduction by controlling dendritic structures, we investigated mechanotransduction in the WT and *Piezo1*$^{-/-}$ OCY454 cells. FSS increased intracellular calcium, activated YAP, and promoted *Cyr61* expression in the WT OCY454 cells, which was abolished by treatment with BAPTA-AM[69], an intracellular calcium chelator, or in *Piezo1*$^{-/-}$ OCY454 cells with dendritic defects (Supplementary Fig. 8e–g, Supplementary Fig. 3b). Disruption of glycocalyx with hyaluronidase, which destabilizes dendritic attachment to the extracellular matrix (ECM) (Supplementary Fig. 8d)[18,70], also abolished FSS-induced YAP activation and *Cyr61* expression (Supplementary Fig. 8e–g) in WT cells. Importantly, CCN1/2 treatment restored osteocyte differentiation and dendrite of the *Piezo1*$^{-/-}$ cells, with partial restoration of calcium influx in response to FSS, which was also abolished by hyaluronidase treatment (Supplementary Fig. 8h, i). Collectively, these data suggest that CCN1/2 control dendrite formation to regulate osteocyte mechanotransduction.

CCNs bind to several cell surface receptors, including integrins[66]. As adhesion molecules linking cells to the ECM, integrins serve central roles in the transduction of mechanical forces via downstream factors such as YAP and integrin-associated proteins such as Src[71–73]. Activated integrin activates Src by inducing Src phosphorylation, which then promotes F-actin reorganization and polymerization[74–76]. To test whether Piezo1 mechanosensing regulates dendrite formation via the YAP-CCN-Src axis, we activated Piezo1 by Yoda1 in WT OCY454 cells and found increased Src phosphorylation, which was abolished by BAPTA-AM (Fig. 7d). CCN1 treatment increased Src phosphorylation, which was more pronounced when CCN1/2 are combined (Fig. 7e). These effects were abolished by dasatinib[77], an inhibitor of tyrosine kinases including Src. Dasatinib treatment directly inhibited dendrite formation (Fig. 7f, Supplementary Fig. 8j). Conversely, overexpression of active Src$^{Y527F}$ increased dendrite number and length in the WT and *Piezo1* cKO cells (Fig. 7g, Supplementary Fig. 8k). Importantly, Src inhibition by dasatinib treatment abolished the rescue effects of CCN1/2 (Fig. 7h, i). Taken together, these results suggest that CCN1/2, downstream of Piezo1 and YAP activation, promote dendrite formation via integrin signaling and Src activation.

During osteocyte differentiation, Src phosphorylation increased progressively with reduced YAP phosphorylation (Supplementary Fig. 8l). As Hippo/YAP signaling is known to interact with Src in several tissues[78,79], we asked whether Src activation may further promote YAP activation downstream of Piezo1 and CCN1/2 activation. In OCY454 cells treated with CCN1/2 conditioned media, Src activation was associated with a strong reduction of YAP phosphorylation and increased total YAP protein (Fig. 7e). Importantly, YAP activation by CCN1/2 treatment was blunted by Src inhibition by dasatinib. Dasatinib treatment increased YAP phosphorylation (Fig. 7j). These results suggest that in response to Src activation by CCN1/2, YAP was further activated via a positive feedforward loop to robustly drive osteocyte maturation and dendrite formation.

### CCN1/2 overexpression rescues osteocyte and bone defects in the *Piezo1*-deficient mice

So far, our data have demonstrated the role of YAP activation in promoting osteocyte dendrite formation and, more importantly, its ability to induce bone gain. Nevertheless, YAP is a key transcription factor regulating many physiological processes with oncogenic potentials in several tissues, such as the skin and liver[80]. The feasibility of direct YAP activation as a therapeutic strategy in combating unloading-induced skeletal disorders is limited. Our in vitro data demonstrate a critical role of CCN1/2 downstream of Piezo1 and YAP in regulating osteocyte dendrite formation. We therefore asked whether increasing circulating CCN1/2 could achieve anabolic effects to rescue bone defects of the *Piezo1* cKO mice. We overexpressed CCN1 and CCN2 in the liver using adeno-associated virus (AAV)[61,81] in WT and *Piezo1* cKO mice (Supplementary Fig. 9a, b). We did not observe changes in body weight, femur length, signs of liver fibrosis or other pathologies (Supplementary Fig. 9c, d). AAV-CCN1/2 rescued cortical but not trabecular bone mass of the *Piezo1* cKO mice (Fig. 8a, b). Consistently, osteocyte dendrites and LCN in the cortical bone, but not trabecular bone, were largely restored to baseline (Fig. 8c, Supplementary Fig. 9f–h). This was accompanied by restored *Sost* and *Spp1* expression levels in the cortical bone, indicating successful morphological and molecular rescue of osteocyte differentiation (Fig. 8d). CCN1/2 did not alter bone mass, dendrites, LCN or osteocyte/osteoblast gene expression in WT mice, suggesting that YAP-CCN signaling may be saturated in normal mice.

Interestingly, overexpression of circulating CCN1/2 increased expression of *Cyr61* in the bone tissue of *Piezo1* cKO mice (Fig. 8e), supporting our in vitro finding where circulating CCN1/2 can further activate YAP via non-cell-autonomous mechanisms, reinforcing the positive feedforward loop in promoting osteocyte differentiation. Elevated *Axin2* and *Lef1* expression due to *Piezo1* loss was restored to control levels by CCN1/2 (Fig. 8f), further supporting that Wnt/β-catenin signaling pathway is likely downstream of the YAP signaling pathway. These data suggest the critical function of CCN1/2 in regulating dendrite formation and bone mass downstream of YAP activation in the cortical bone, as well as their potential as a druggable target in treating loading/unloading induced skeletal pathologies such as osteoporosis.

## Discussion

Osteocytes comprise >90% of bone cells and play a major role in mediating mechanical stimulation in regulating bone formation[82]. Osteocyte maturation is characterized by drastic morphological changes, forming a dendritic network. Osteocytes experience continuous mechanical input from FSS within the LCN and the tethering elements connecting cells to the LCN, which result from macroscopic loading on the bone[83]. The dendritic network amplifies small matrix deformations, leading to enhanced mechano-stimulation on osteocytes[84], which are collectively determined by the magnitude and duration of loading, bone matrix properties and LCN microstructure[85,86]. Previous studies have demonstrated the critical role of Piezo1 in osteocyte mechanotransduction. Changes in bone mass due to unloading/loading are mitigated when *Piezo1* is removed

https://doi.org/10.1038/s41467-025-65636-9

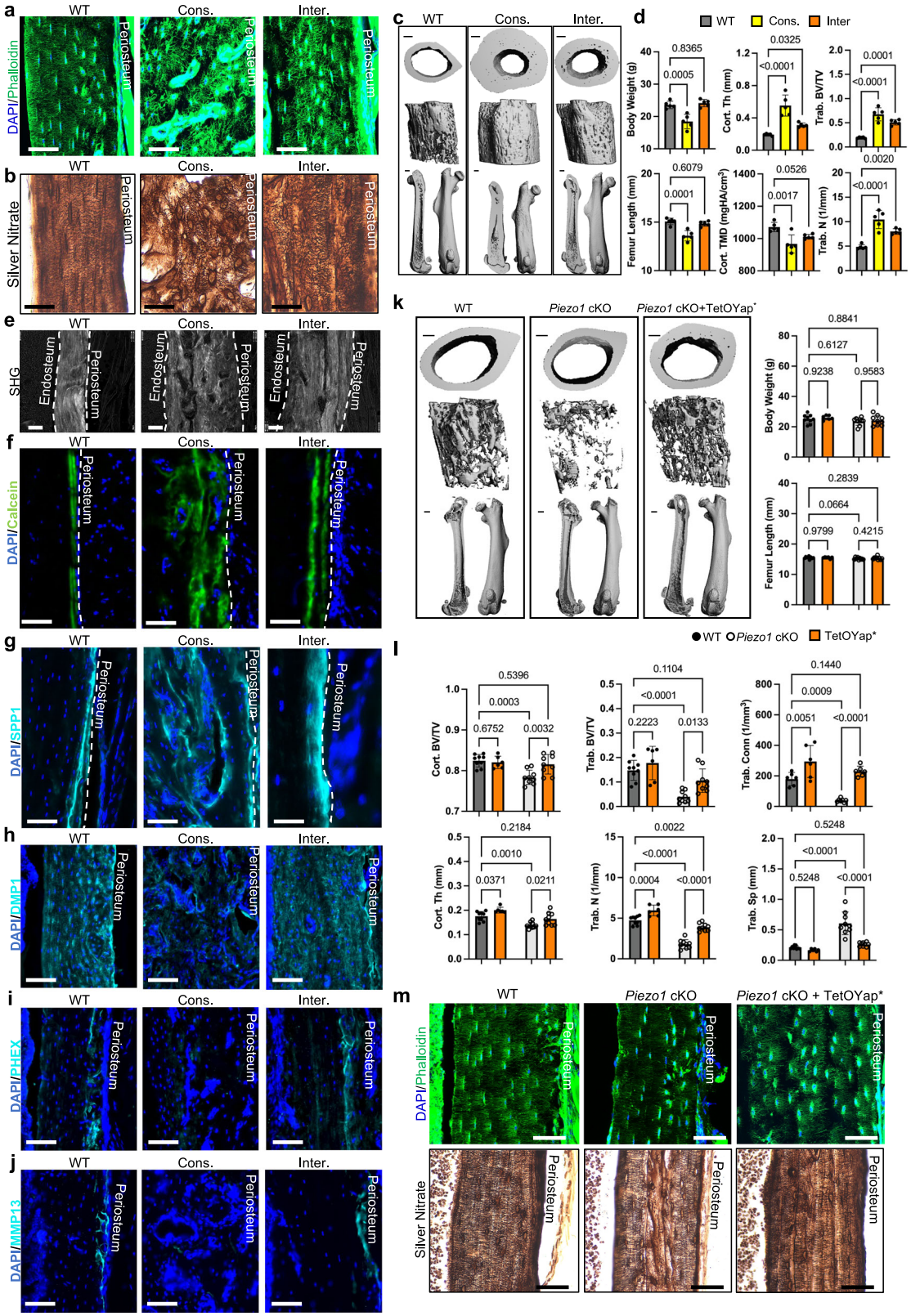


from osteoblasts/osteocytes[10–12]. In this study, we show that Piezo1 is critical in the acquisition of osteocyte identity and morphology in its development, which may serve to amplify the ability of osteocytes to sense mechanical stimulation in regulating bone formation and resorption. Thus, Piezo1 is required to enable osteocytes to respond efficiently to mechanical stimulation. Importantly, the role of Piezo1 in osteocytes is also non-cell autonomous, as we identify that its function can be mediated by secreted factors, CCN1 and CCN2. Piezo1 activation likely acts through a positive feedforward mechanism via YAP activation and CCN1/2 expression to promote osteocyte maturation and dendritic network formation, both of which are required for normal bone homeostasis.

Many of the regulatory genes expressed in osteocytes are transcriptionally controlled by mechanical stimuli. While mineralization

**Fig. 5 | Intermittent YAP activation rescues dendritic and bone defects in the *Piezo1*-deficient mice. a** Phalloidin staining (green; nucleus: blue) of dendritic network, quantified in Supplementary Fig. 6c ($N = 3$ biological replicates), and **b** silver nitrate staining of LCN, quantified in Supplementary Fig. 6d ($N = 3$ biological replicates), in *Dmp1Cre; TetOYAP*$^{+}$ (YAP gain) mice subjected to constant (cons.) or intermittent (inter.) YAP activation for 5-weeks. Mice were collected at 8-weeks-old. **c**, **d** μCT analysis of femur cortical and trabecular bone in YAP gain mice. $N = 5$ biological replicates. **e** Second harmonic generation (SHG, white) imaging of femur midshaft cortical bone in WT and YAP gain mice. $N = 3$ biological replicates. **f** Dynamic histomorphometry analysis of femur midshaft cortical bone, quantified in Supplementary Fig. 6f. $N = 5$ biological replicates. Calcein (green; nucleus: blue) was injected at 8 and 2 days before collection at 8-week-old. **g**–**j** IF staining of SPP1, DMP1, PHEX, and MMP13 (cyan; nucleus: blue) in WT and YAP Gain mice, quantified in Supplementary Fig. 6i, j. $N = 3$ biological replicates. **k**, **l** μCT analysis of femur cortical and trabecular bone in WT and *Piezo1* cKO mice treated with YAP gain. Mice were treated with intermittent Dox for 5 weeks and collected at 12-weeks old. $N = 9$ (WT, *Piezo1* cKO and *Piezo1* cKO with YAP gain) and 6 (WT with YAP gain) biological replicates. **m** Phalloidin (green; nucleus: blue) and silver nitrate staining of femur cortical midshaft in WT, *Piezo1* cKO, and *Piezo1* cKO with YAP gain mice, quantified in Supplementary Fig. 6o, r. $N = 3$ biological replicates. Scale bar: **a**,**b**, **e**–**j**, **m** 50 μm, **c**, **k** 100 μm. Bar graphs represent mean ± SD. **d** one-way ANOVA with Holm-Sidak's post-hoc correction. **k**, **l** Two-way ANOVA using *Piezo1* cKO and YAP gain as independent variables. Holm-Sidak's post-hoc correction was performed to compare group differences. Source data are provided as a Source Data file.

and mechanical loading promote *Dmp1* and *Sost* expression in osteocytes[87–89], mechanical loading of mature osteocytes robustly suppresses *Tnfsf11* and *Sost* expression[47,90] to reduce bone resorption while promoting bone formation. We observed progressive osteocyte maturation and dendrite formation from the periosteal side in postnatal bone development, which correlated to bone matrix stiffening in the normal bone, suggesting that Piezo1 may be progressively activated during osteocyte differentiation and dendrite formation. Indeed, reductions in dendrite and LCN due to *Piezo1* loss were more significant on the endosteal side. Consistently, YAP activation or CCN1/2 overproduction increased dendrite and LCN on both sides, with more significant effects on the periosteal side, suggesting that the newly embedded osteocytes are more susceptible to regulation by YAP-CCN1/2 activation. Higher YAP activities or CCN1/2 doses may be required to correct the endosteal osteocyte defects. While we find a correlation between increased roundness and differentiation defects in *Piezo1*-deficient mice, changes in cell shape may not always reflect differentiation status, as these two processes may be regulated distinctly.

It is surprising that Wnt/β-catenin signaling, which promotes bone formation, was increased in the *Piezo1 c*KO bone, likely due to reduced *Sost* expression, caused by reduced YAP activation. Our observation of continuous down-regulation of Wnt/β-catenin signaling associated with osteocyte maturation is consistent with upregulation of *Sost* expression in this process and our previous findings that sustained Wnt/β-catenin activation inhibits osteoblast maturation and terminal mineralization[91–93]. Our findings support an interesting scenario that while Wnt activation is required for osteoblastic differentiation, inhibition of Wnt is required for maturation from osteoblasts to osteocytes. Our data further suggest that Wnt/β-catenin signaling pathway is likely downstream of YAP regulation by Piezo1, as intermittent YAP activation and CCN1/2 overexpression reduced the elevated *Axin2* and *Lef1* expression caused by Piezo1 deficiency. YAP may bind to β-catenin to inhibit its transcriptional activities[94]. YAP can also reprogram cancer stem cells into a low Wnt, non-proliferative state[95]. We show that YAP activation promotes *Sost* expression during osteocyte maturation, and SOST is a secreted inhibitor of Wnt/β-catenin[59]. CCN1/2 overexpression can promote YAP activation via a positive feedback loop and may therefore inhibit Wnt signaling via a similar mechanism.

Recently, it was reported that expression of *Wnt1*, expressed in osteocytes and required for osteoblast differentiation[96], was down-regulated in *Piezo1* cKO mice[10]. While we also found a trend of reduced *Wnt1* expression in *Piezo1* cKO mice (Supplementary Fig. 3n), expression of *Axin2* and *Lef1* was increased in vitro and in vivo, indicating upregulation of the Wnt/β-catenin signaling activity. The Wnt signaling pathway is dynamically regulated by Wnt ligands, Wnt receptors and other regulators such as secreted activators and inhibitors, including R-spondins, Dickkopfs, and Secreted Frizzled Related Proteins. Further investigation is needed to determine the cellular and molecular mechanism whereby Wnt/β-catenin signaling is activated by loss of Piezo1 during osteocyte differentiation.

Mechanical force stimulates the formation of stress fibers, which activate YAP and TAZ in the Hippo signaling pathway[33]. YAP in turn controls cytoskeleton dynamics, regulating cell morphology and migration. YAP/TAZ deletion impairs osteocyte dendritic and LCN[32], supporting our finding on the important role of YAP/TAZ in mediating the Piezo1-dependent function in the formation of osteocyte dendritic network. In this work, we further demonstrated that forced intermittent YAP activation, in the absence of Piezo1, drove cellular and molecular maturation of osteocytes, demonstrating that YAP/TAZ activation is both necessary and sufficient to mediate the function of Piezo1 in osteocyte maturation and dendrite formation. Importantly, intermittent YAP activation in the *Piezo1* KO osteocytes not only rescued dendritic defects, cortical and trabecular bone loss associated with Piezo1 deficiency was also completely rescued. Our studies also highlight a drastic difference between constant and intermittent YAP activation in controlling normal bone formation (Fig. 5a–j). Despite increased bone mass, constant YAP activation impaired bone quality and inhibited osteocyte differentiation in addition to disrupting the dendrite network, which possibly mimics excessive loading that induces pathological woven bone formation[97]. In contrast, intermittent YAP activation promoted normal lamellar bone formation with enhanced osteocyte differentiation and dendritic network formation, similar to physiological moderate cyclic loading. Whether intermittent TDI-011536 treatment or periodic Dox feeding indeed recapitulates physiological cyclic loading requires further investigation. Our findings demonstrate that dynamic YAP activation is critical in controlling normal bone and osteocytes.

Dendrite formation involves cytoskeletal remodeling with F-actin reorganization. YAP activation, inhibition of Wnt/β-catenin, or CCN1/2 expression, all promoted osteocyte maturation and dendrite formation, suggesting that they may act in the same pathway. Indeed, it is known that YAP and Wnt/β-catenin signaling can antagonize each other[94,98], while CCN1/2 are well-known canonical downstream targets of YAP[49] and can act through integrins, their most extensively documented CCN-binding receptors[66], which can activate Src and promote YAP activation[33,73,99]. Our in vitro and in vivo findings led us to propose a YAP-CCN1/2-Src axis as a critical pathway in controlling mechanical loading-induced dendrite formation during the maturation from osteoblasts to osteocytes (Fig. 8g). Nuclear translocation of YAP induced by Piezo1 activation upregulates transcription of late osteoblast and osteocyte-specific genes such as *Dmp1* and *Sost*, as well as canonical YAP target genes *Cyr61* and *Ctgf*. Secreted CCN1/2 proteins bind to membrane integrin receptors, activating Src and thereby promoting actin polymerization and dendrite formation through both cell-autonomous and non-cell-autonomous mechanisms. This Src activation and actin polymerization further promote YAP activation, creating a positive feedforward loop that drives osteocyte maturation. On the other hand, SOST secretion antagonizes Wnt/β-catenin signaling to further enhance osteocyte maturation and dendrite formation. In this regard, circulating CCN1 and CCN2 may be promising therapeutic targets for bone defects caused by underloading.

https://doi.org/10.1038/s41467-025-65636-9

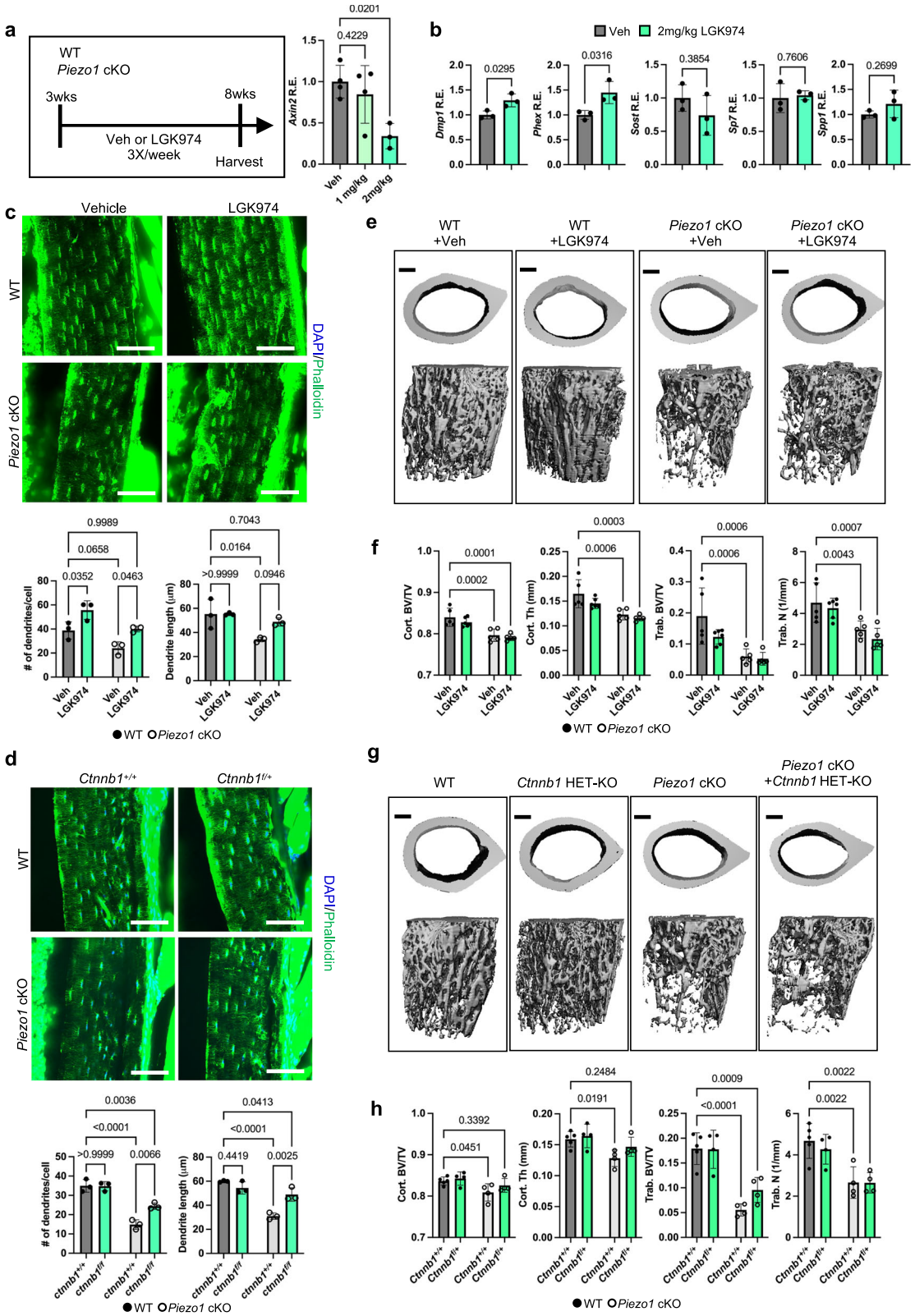


A critical finding from our studies is the identification of CCN1/2 as secreted factors that mediate osteocyte maturation and bone mass control. Past studies have shown that CCN1 and CCN2 promote osteoblastic differentiation cell-autonomously by inducing osteoblastic gene expression and promoting mineralization, respectively[100]. Osteoblast-specific deletion of CCN1 using *Osteocalcin-Cre* reduced bone mineral density and trabecular bone mass[100]. Our studies reveal the intriguing finding that CCN1/2 may serve as critical bone-secreted regulatory factors in response to mechanical loading that act non-cell-autonomously in bone and potentially other organs too. Osteocytes can non-cell-autonomously control bone homeostasis via multiple strategies, such as secreted factors and the dense network of dendrites. Despite the anabolic effects of intermittent genetic YAP activation, targeting YAP as a therapeutic strategy for managing loading/

**Fig. 6 | Wnt inhibition rescues dendritic defects in the *Piezo1*-deficient mice.** **a** Schematic of low-dose LGK974 treatment and *Axin2* expression measured by qRT-PCR analysis of bone tissue 6 h after LGK974 treatment. $N = 4$ (Vehicle and 1 mg/kg LGK974) and three (2 mg/kg LGK974) biological replicates. **b** qRT-PCR analysis of osteocyte (*Dmp1*, *Phex*) and osteoblast (*Sp7*, *Spp1*) marker genes in cortical bone tissue 6 h after 2 mg/kg LGK974 treatment. $N = 4$ biological replicates. **c** Phalloidin staining (green; nucleus: blue) and osteocyte dendrite quantification of femur midshaft cortical bone in WT and *Piezo1* cKO mice treated with LGK974 for 5 weeks. Mice were collected at 8-weeks old. $N = 3$ biological replicates. **d** Phalloidin staining (green; nucleus: blue) and osteocyte dendrite quantification of femur midshaft cortical bone in WT and *Piezo1* cKO mice with 1 copy of *β-catenin* deletion (*Ctnnb1*$^{f/+}$). $N = 3$ biological replicates. **e**, **f** μCT analysis of femur cortical and trabecular bone in LGK974-treated WT and *Piezo1* cKO mice. $N = 5$ (WT, *Piezo1* cKO, *Piezo1* cKO treat with LGK974) and 6 (WT treated with LGK974) biological replicates. **g**, **h** μCT analysis of femur cortical and trabecular bone in 8-week-old WT and *Piezo1* cKO mice with *Ctnnb1*$^{f/+}$. $N = 5$ (WT) and 4 (*Piezo1* cKO, *Ctnnb1* HET-KO, and *Piezo1* cKO with *Ctnnb1* HET-KO) biological replicates. Scale bar: **c**, **d** 50 μm, **e**, **g** 200 μm. Bar graphs represent mean ± SD. **a** one-way ANOVA with Holm-Sidak's post-hoc correction. **b** Two-sided unpaired Student's *t* test. **c**, **d**, **f**, **h** Two-way ANOVA using *Piezo1* cKO and LGK974/*Ctnnb1*$^{f/+}$ as independent variables. Holm-Sidak's post-hoc correction was performed to compare group differences. Source data are provided as a Source Data file.

unloading-induced pathologies such as osteoporosis poses risks, as excessive YAP activation is oncogenic[80]. We show that targeting the secreted elements CCN1/2 downstream of YAP may be a promising alternative strategy. While hepatocyte CCN1 overexpression has been shown to aggravate liver fibrosis and steatosis[101,102], delivery of CCN1/2 via viral vectors to the mouse liver did not induce fibrosis and steatosis, suggesting that it is possible to optimize the anabolic effects on bone while minimizing liver side effects.

We realize several limitations of the current study. Examination of tdTom expression in our hands demonstrated that in the adult (8-week-old) mice, while tdTom expression was restricted to cortical and trabecular osteoblast/osteocytes in postnatal bone (Fig. 3j–l), tdTom was also found in the skeletal muscle (Supplementary Fig. 2a). Nevertheless, studies with new genetic tools with more precise cell specificities are needed to further dissect the role of Piezo1 and YAP/TAZ in osteocytes. Another limitation is that while overexpression of CCN1/2 fully restored cortical bone mass, trabecular bone loss was not rescued. Our data show that trabecular bone osteocyte dendrites are also regulated by Piezo1 and YAP. However, downstream of YAP, CCN1/2 may not be the major factors regulating trabecular bone osteocyte differentiation and/or dendrite formation. Regarding the in vitro studies, it is important to note that the culture environment differs significantly from the native bone tissue. As a result, the precise molecular mechanisms underlying cytoskeleton reorganization during dendrite outgrowth may vary considerably. Furthermore, systemic CCN1/2 may influence other signaling processes or even impact other cell types, and hyaluronidase may also affect other signaling pathways in osteocytes. Although we show that the Piezo1-YAP-CCN1/2-mediated mechanotransduction critically regulates osteocyte maturation and dendrite formation, the precise contribution of restored dendritic structure in rescuing bone mass remains unclear. The mechanistic regulation of bone mass by mechanotransduction is complex, involving both osteoblasts and osteocytes. While the integrity, proper alignment and polarity of osteocyte dendrites may contribute to this process, it may not be the only mechanism. Distinguishing dendrite-specific regulations and identifying the precise cellular targets of CCN1/2 remain important, which is a subject for future investigation with newly developed genetic and molecular tools. Despite these limitations, our studies uncover mechanistic insights into the essential roles of Piezo1 and the YAP-CCN1/2-Src signaling axis in controlling osteocyte maturation and dendrite formation. Our findings reveal CCN1/2 as promising targets for robust control of osteocyte dendritic network formation and bone mass.

# Methods

## Mouse lines

All animal experiments were conducted in accordance with protocols approved by the Harvard Medical School Institutional Animal Care and Use Committee. Mice were housed in a pathogen-free facility with a 12-h light/dark cycle. Both male and female mice were used, with gender-matched littermates carrying negative genotypes serving as controls. Mice described in the literature and purchased from the Jackson Laboratories: *Piezo1*$^{f/f}$ (stock# 029213), *Dmp1-Cre* (stock# 023047), *Rosa26-TdTomato* (stock# 007909), *Axin2-mGFP* (stock# 037313), *Sox9-CreER* (stock# 035092), *Ctnnb1*$^{f/f}$ (stock# 004153). Long bones from *Sost-KO* mice are kindly provided by Dr. X. Edward Guo's laboratory at Columbia University. *TetOYAP*$^{s}$ (*Rosa26*$^{lox\text{-}stop\text{-}lox\text{-}rtTA/+}$; *Col1a1*$^{Teto\text{-}YAPS127A}$)[61] mice were provided by Dr. Fernando D. Camargo's laboratory. In these mice, YAP activation was achieved by activating expression of a Dox-inducible version of human YAP carrying an S127A mutation, which cannot be inactivated by LATS1/2 and has enhanced nuclear localization.

## Immunofluorescent staining

Postnatal and adult specimens were fixed in 4% paraformaldehyde (PFA) in phosphate-buffered saline (PBS). After equilibration in 15% and 30% sucrose in PBS, samples were embedded in O.C.T. compound for cryosectioning. Sections (12–30 μm thick) were permeabilized and blocked in 10% donkey serum/0.5% Triton X-100 in PBS for 1 h at room temperature. Primary antibodies were incubated overnight at 4 °C, followed by secondary antibodies at room temperature for 30 min. Autofluorescence was quenched using the TrueVIEW Autofluorescence Quenching Kit before mounting. Sections were imaged with a fluorescent or confocal microscope, and images were quantified using ImageJ.

## Staining and quantification of osteocyte dendrite and canalicular network

For F-actin visualization, 30-μm sections were permeabilized in 0.5% Triton X-100 in PBS for 1 h and incubated with phalloidin for 1 h at room temperature. Confocal microscopy was used to acquire images, with 5-μm z-stacks collected at 0.5 μm intervals. Images were collected using the Leica DMi8/Stellaris 8 Falcon microscope with Leica LAS X software. Canalicular networks were visualized using silver nitrate staining on 8–10 μm sections using a Keyence BZ-X710 microscope. Dendrite number/length and canalicular number/length were quantified using ImageJ, and dendrite orientation distribution was analyzed with the OrientationJ Plugin in Fiji. For 3D collagen gel cultures, gels were fixed in 4% PFA in PBS, permeabilized, and stained with phalloidin. Whole-mount fluorescent images were acquired with a fluorescent microscope at 10×. High-resolution images of osteocyte dendrites were acquired with a confocal microscope at 20–40× to perform quantification of dendrite number and length.

## Bone microindenation

Microindentation was performed following previously published procedures in Dr. X. Edward Guo's laboratory at Columbia University[103,104]. Freshly dissected femurs from 6-week-old WT mice were collected. Bone ends were removed to remove bone marrow completely. Cortical bone pieces were left to dry completely for 30 min before embedding in plastic resin. After complete curing of the plastics, embedded bone tissue was cut using a slow-speed saw and polished to expose transverse and longitudinal sections for microindentation. Indentation was performed using a custom-built microindentation machine and a light

https://doi.org/10.1038/s41467-025-65636-9

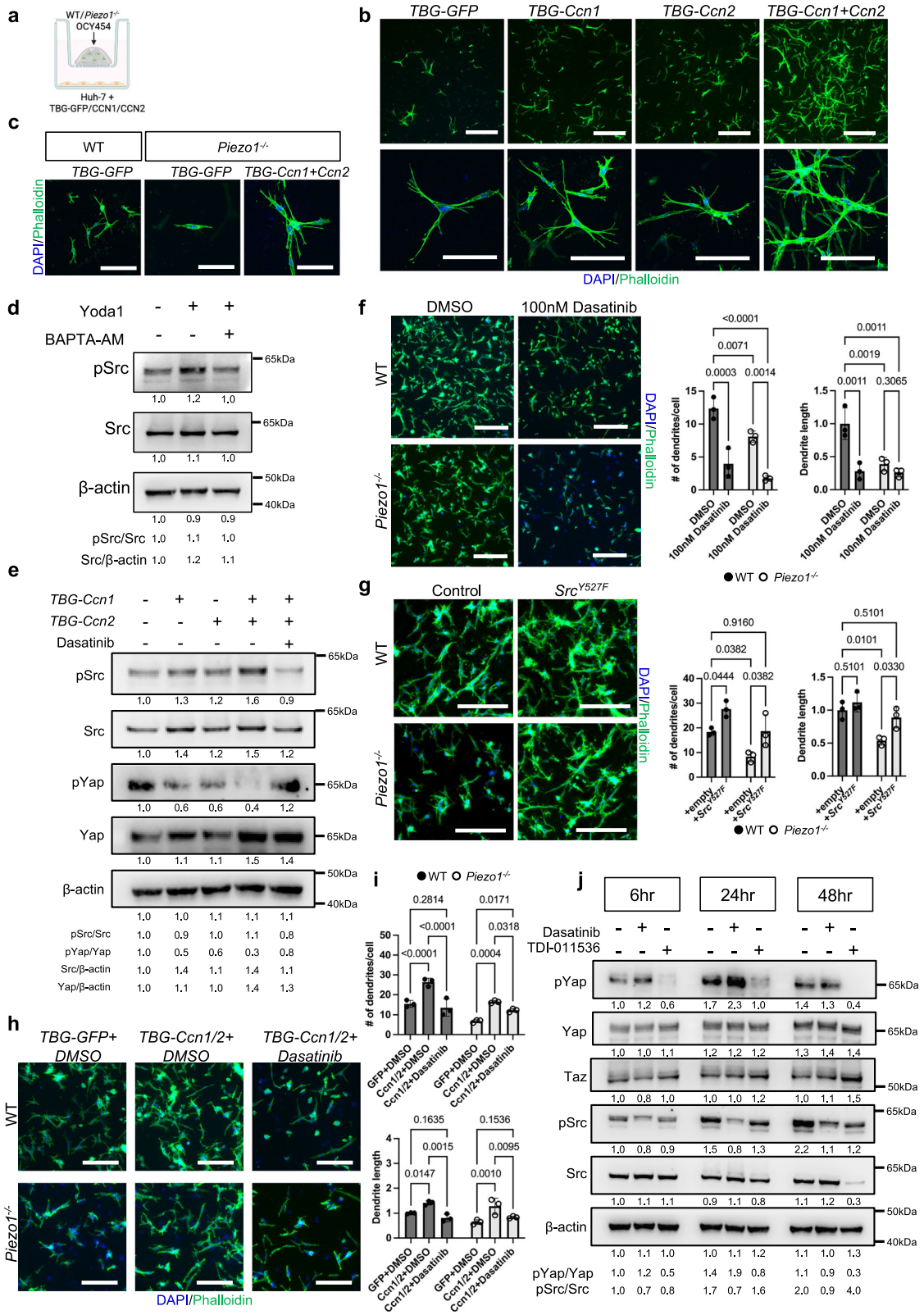


microscope on a 2-axis linear translation stage. A cylindrical indenter with a diameter of 25 µm (National Jet Co., Inc.) was used. Samples were preloaded to a displacement of 2.5 µm, unloaded to 0.25 µm, reloaded to a depth of 2.5 µm, and unloaded completely at a monotonic rate of 50 nm/s. Young's modulus was calculated from the initial portion of the unloading curve, where the deformation of the tested sample and indenter is assumed to be purely elastic[105]. Samples were kept hydrated by gentamicin solution throughout the indentation procedure. Paired sites on the endosteal and periosteal sides of the cortical bone were identified under the light microscope. Indents were performed on transverse cross-sections to determine axial elastic modulus and on longitudinal cross-sections to determine transverse elastic modulus.

**Fig. 7 | Piezo1 promotes dendrite formation via activation of the YAP-CCN1/2-Src signaling axis. a** Schematic of OCY454 cells in 3D hydrogels co-cultured with Huh-7 cells. Created in BioRender. Hu, Y. (2025) https://BioRender.com/4k88lcq. **b** Phalloidin staining (green; nucleus: blue) of WT OCY454 cells co-cultured with GFP/CCN1/CCN2-expressing Huh-7 cells for 5 days, quantified in Supplementary Fig. 8a. $N = 5$ independent experiments. **c** Phalloidin staining (green; nucleus: blue) of *Piezo1*$^{-/-}$ OCY454 cells co-cultured with Huh-7 cells overexpressing CCN1 and CCN2 for 5 days, quantified in Supplementary Fig. 8b. $N = 5$ independent experiments. **d** WB analysis of pSrc and Src levels in WT OCY454 cells treated with 1 μM Yoda1 and 10 μM BAPTA-AM for 24 h. Experiment was repeated three times with similar results. Representative data from 1 experiment is shown. **e** WB analysis of pSrc, Src, pYAP and YAP levels in WT OCY454 cells after 6-h treatment with conditioned media from Huh-7 cells overexpressing CCN1/CCN2 and 100 nM dasatinib. Experiment was repeated three times with similar results. Representative data from one experiment is shown. **f** Phalloidin staining (green; nucleus: blue) and dendrite quantification of WT and *Piezo1*$^{-/-}$ OCY454 cells treated with 100 nM dasatinib for 3 days. $N = 3$ independent experiments. **g** Phalloidin staining (green; nucleus: blue) and osteocyte dendrite quantification of WT and *Piezo1*$^{-/-}$ OCY454 cells over-expressing Src$^{Y527F}$ cultured for 3 days. $N = 3$ independent experiments. **h, i** Phalloidin staining (green; nucleus: blue) and osteocyte dendrite quantification of WT and *Piezo1*$^{-/-}$ OCY454 cells co-cultured with Huh-7 cells overexpressing CCN1 and CCN2 treated with 100 nM Dasatinib for 3 days. $N = 3$ independent experiments. **j** WB analysis of pYAP, YAP, TAZ, pSrc, and Src levels in WT OCY454 cells treated with 100 nM Dasatinib or 300 nM of TDI-011536 for the indicated durations. Experiment was repeated three times with similar results. Representative data from one experiment is shown. Bar graphs represent mean ± SD. Scale bar: (**b**, **c**, **f**–**h**) 100 μm. **f**, **g**, **i** one-way ANOVA with Holm-Sidak's post-hoc correction. Source data are provided as a Source Data file.

### Cell culture

Ocy454 cells express a thermosensitive large T antigen, active at 33 °C and inactive at 37 °C. Cells were cultured in alpha-minimum essential medium (MEM) with 10% fetal bovine serum and 1% antibiotic-antimycotic (Gibco) at 33 °C in collagen-coated dishes. Osteocyte differentiation was induced by shifting to 37 °C. For 2D cultures, cells were grown in collagen-coated 12-well plates and media was replaced every 3 days. For 3D cultures, rat tail collagen I (Advanced Biomatrix) was mixed with a neutralization buffer at a 9:1 ratio on ice. The cell suspension (final concentration of $10^5$ cells/mL) was mixed with culture media and buffered collagen and then plated in 24-well plates. Gels were cured at 37 °C for 1 h before adding culture media. Transfections were performed using PEI MAX (Polysciences, Inc.). For transwell cultures, Huh-7 cells were plated, transfected with *TBG-GFP*, *TBG-CCN1*, or *TBG-CCN2*, and then co-cultured with OCY454 cell suspensions in hanging inserts. To investigate the effects of matrix stiffening, OCY454 cells were seeded in 3D collagen hydrogels containing a higher concentration of rat tail collagen I that increased gel stiffness by two-fold (Advanced Biomatrix). For FSS experiments, OCY454 cells in 3D collagen gels were seeded in 6-well plates with 3 mL of culture media in each well. FSS was performed using an orbital shaker at 150 rpm. Cells were stimulated for 1 h each day for a total of 3 days. For intracellular calcium imaging, cells were incubated with Fluo8-AM (AAT-Bioquest) for 1 h before FSS stimulation. Time-lapse imaging was captured for 1 min at 2- or 5-s immediately after FSS stimulation. For hyaluronidase treatment, osteocytes were first differentiated for 3 days to allow dendrites to form. Hyaluronidase (STEMCELL Technologies) was then dissolved in PBS and added to cells at 250 U/mL for 1 h at 37 °C[18].

### Generation of Piezo1$^{-/-}$ Ocy454 cell line

CRISPR/Cas9 was used to delete *Piezo1* in Ocy454 cells. Guide RNAs targeting exons 19 and 23 of the *Piezo1* gene were subcloned into pSpCas9(BB)-2A-Puro (PX459, Addgene Plasmid #62988). Control cells were generated using the PX459 backbone without gRNA. Ocy454 cells were co-transfected with the targeting plasmids and selected for single-cell clones. PCR and Sanger sequencing confirmed one clone with bi-allelic deletion of *Piezo1*. This clone was used as the *Piezo1*$^{-/-}$ Ocy454 line. To verify CRISPR/Cas9 specificity, *Piezo1*$^{-/-}$ Ocy454 cells were transfected with mPiezo1-IRES-eGFP (Addgene Plasmid #80925) and cultured in 3D collagen gel with Neomycin selection. Cells transfected with PcDNA3.1 (Neomycin resistance) were used as controls. After 10 days, 3D cultures were processed for phalloidin staining.

### Small molecule treatment

For in vitro experiments, Yoda1 (1 μM)), TDI-011536 (300 nM–1 μM), verteporfin (50–200 nM), CHIR99021 (500 nM), LGK974 (500 nM), and Dasatinib (100 nM) were added to the culture media. For in vivo treatment, LGK974 (2 mg/kg) was administered to 3-week-old mice by oral gavage three times a week until the mice were 8 weeks old.

### Genetic YAP activation

YAP was activated genetically by supplementing doxycycline (0.2 g/L) with sucrose (25 g/L) in the drinking water of YAP gain mice. For mice collected at 8 weeks old, Dox was administered constantly or intermittently (7 days on/7 days off) for 5 weeks, starting from 3 weeks old. For mice collected at 12 weeks old, Dox was administered intermittently (5 days on/9 days off) for 8 weeks from 3 weeks old. Littermates lacking the YAP gain gene served as controls.

### μCT analysis

Femurs were harvested, fixed overnight in 4% PFA, and stored in 1X PBS. The femurs were imaged using a desktop μCT35 (Scanco Medical) at a 12 μm voxel size, 55 kV energy, 145 μA current, and 8 W power. Trabecular bone was analyzed in a 200-slice region immediately beneath the growth plate for trabecular bone volume fraction (Trab. BV/TV), number (Trab. N), thickness (Trab. Th), and connectivity (Trab. Conn). Cortical bone was analyzed in a 100-slice region at the midshaft femur for cortical bone volume fraction (Cort. BV/TV) and thickness (Cort. Th).

### Western blotting

Cell lysates were prepared in RIPA buffer (Santa Cruz Biotechnology) containing Protease Inhibitor Cocktail (PIC) and PhosSTOP (Roche). Protein concentrations were quantified by the BCA protein assay kit (Thermo Fisher Scientific). Equal amounts of protein were resolved by SDS-PAGE and further transferred to the Nitrocellulose Blotting Membrane (Cytiva). Target proteins were detected with the Super-Signal West Pico Plus Chemiluminescent Substrate (Thermo Fisher Scientific) using the PXi4 Chemiluminescent Imaging System (Syngene). Antibodies used are listed in Supplementary Table 2.

### QRT-PCR analysis

Total RNA was extracted using QIAzol Lysis Reagent (QIAGEN). For in vitro cultures, cells were lysed directly in the culture dish. For bone tissues, freshly dissected limbs were cleaned of muscle and connecting tissues, and bone marrow was removed. Bones were stored in RNAlater solution (Thermo Fisher Scientific) before homogenization and RNA extraction. First-strand cDNA was synthesized using SuperScript II Reverse Transcriptase (Life Technologies) with random primers. QRT-PCR was performed with SYBR Select Master Mix on a StepOnePlus Real-Time PCR System (Thermo Fisher Scientific). Gene expression levels were normalized to glyceraldehyde 3-phosphate dehydrogenase (GAPDH) by calculating the ΔCt values relative to GAPDH. ΔΔCt was then calculated by normalizing ΔCt values of the experimental groups to the control group. Primer sequences used for qRT-PCR analyses are listed in Supplementary Table 3. Primers were generated commercially by Integrated DNA Technologies.

### RNA sequencing

WT and *Piezo1*$^{-/-}$ OCY454 cells differentiated for 1, 14, and 28 days were processed for RNA sequencing with two replicates per group. DNA was

https://doi.org/10.1038/s41467-025-65636-9

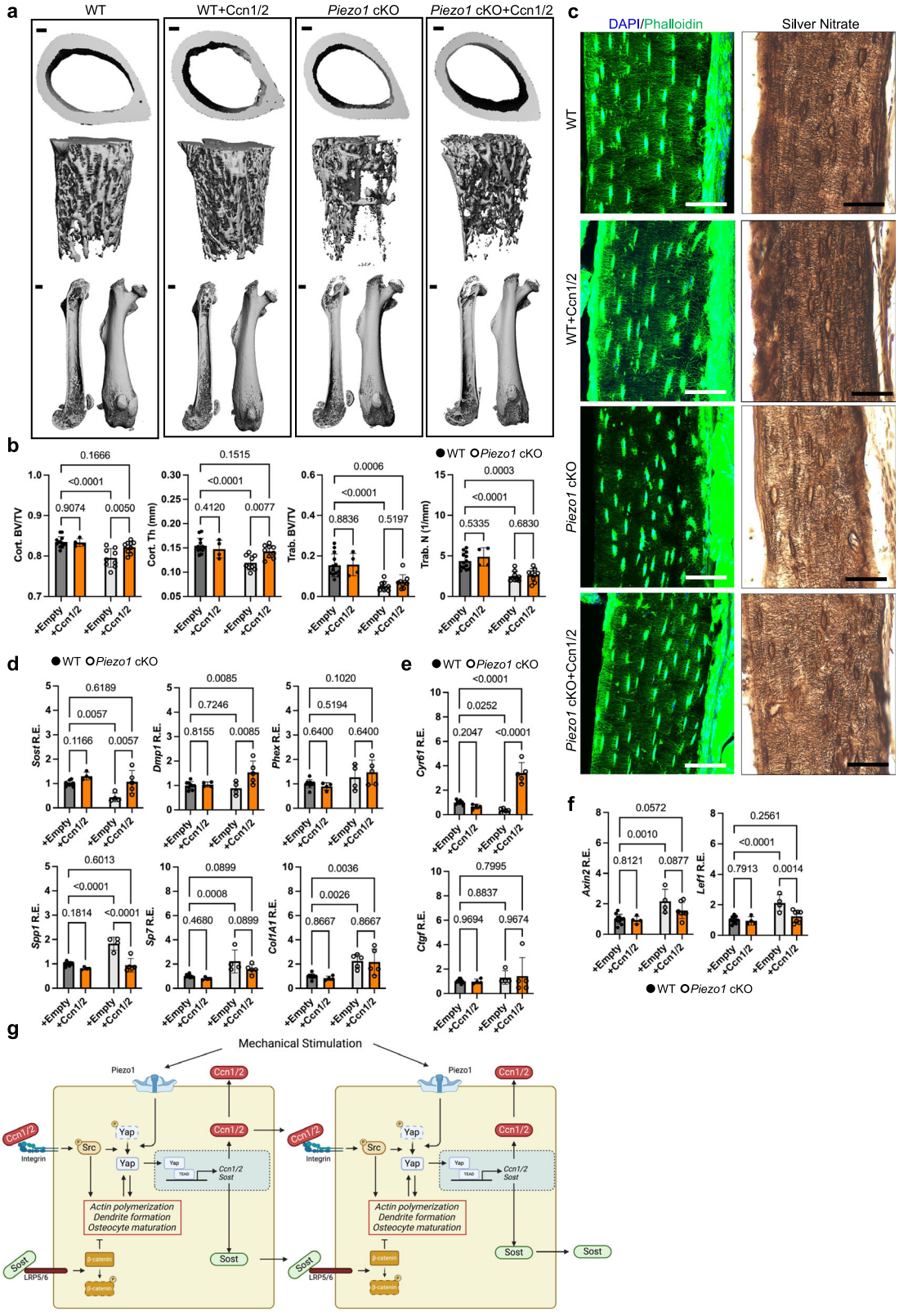


removed from RNA using a RapidOut DNA Removal Kit (Thermo Fisher Scientific) according to the manufacturer's instructions. 400–1000 ng RNA sample reaction was used for mRNA isolation using an NEBNext Poly(A) mRNA Magnetic Isolation Module (New England Biolabs). Libraries were prepared using an xGen RNA Library Prep Kit (IDT) according to the manufacturer's instructions. Barcoded libraries were sequenced on an Illumina NextSeq 550/1000 at the Genomics Technology Laboratory of NCI. Paired-end sequencing mode (2 × 45 bp) was used in the experiments. Samples were sequenced with two replicates for each condition and time point.

### Computational analysis of bulk RNA-seq data

Raw counts were normalized, and differential expression analysis was performed using the edgeR package[106]. Heatmaps were generated

**Fig. 8 | CCN1/2 overexpression rescued osteocyte and bone defects in the *Piezo1*-deficient mice. a**, **b** μCT analysis of femur cortical and trabecular bone of WT and Piezo1 cKO mice treated with AAV-Empty or AAV-CCN1/2 at 3-weeks old. Mice were collected at 8-weeks old. $N = 13$ (WT + AAV-Empty), 4 (WT + AAV-CCN1/2), and 9 (*Piezo1* cKO + AAV-Empty and *Piezo1* ckO + AAV-CCN1/2) biological replicates. **c** Phalloidin (green; nucleus: blue) and silver nitrate staining of femur cortical bone in WT and *Piezo1* cKO mice treated with AAV-Empty or AAV-CCN1/2, quantified in Supplementary Fig. 9f, g. $N = 3$ biological replicates. **d** Expressions of osteocyte (*Sost*, *Dmp1*, *Phex*) and osteoblast (*Sp7*, *Col1A1*, *Spp1*) markers, **e** YAP (*Cyr61*, *Ctgf*) target genes, and **f** Wnt/β-catenin (*Axin2*, *Lef1*) target genes measured by qRT-PCR analysis of cortical bone of WT and *Piezo1* cKO mice treated with AAV-Empty or AAV-CCN1/2. $N = 9$ (WT + AAV-Empty), 4 (WT + AAV-CCN1/2, *Piezo1* cKO), and 5 (*Piezo1* ckO + AAV-CCN1/2) biological replicates. **g** Proposed schematic of Piezo1-mediated YAP-CCN1/2-Src signaling axis in osteocyte mechanotransduction. Nuclear translocation of YAP induced by Piezo1 activation upregulates transcription of late osteoblast and osteocyte-specific genes such as *Dmp1* and *Sost*, as well as canonical YAP targets CCN1 (*Cyr61*) and CCN2 (*Ctgf*). Secreted CCN1/2 proteins bind to membrane integrin receptors, activating Src and thereby promoting actin polymerization and dendrite formation through both cell-autonomous and non-cell-autonomous mechanisms. This Src activation and actin polymerization further promote YAP activation, creating a positive feedforward loop that drives osteocyte maturation. On the other hand, SOST secretion antagonizes Wnt/β-catenin signaling to further enhance osteocyte maturation and dendrite formation. Created in BioRender. Hu, Y. (2025) https://BioRender.com/6ma05x9. Scale bar: **a** 100 μm, (**c**) 50 μm. Bar graphs represent mean ± SD. **b**–**f** Two-way ANOVA using *Piezo1* cKO and AAV-*CCN1/2* treatment as independent variables. Holm-Sidak's post-hoc correction was performed to compare group differences. Source data are provided as a Source Data file.

using the "pheatmap" function in the R software or the "Morpheus" web tool (https://software.broadinstitute.org/morpheus/). Gene ontology analysis was performed using the "ClusterProfiler"[107]. GSEA was performed using a one-sided Kolmogorov–Smirnov–like running-sum statistic with phenotype-based permutation testing and false discovery rate (FDR) correction for multiple comparisons. KEGG functional analysis was performed using "ClusterProfiler".

### AAV injection

AAV8 vectors encoding mouse CCN1 or CCN2 under the control of the TBG promoter (pAAV8-TBG-CCN1 and pAAV8-TBG-CCN2) were generated in the laboratory. The AAV viruses were diluted in sterile PBS and administered via retro-orbital injection to 3-week-old WT or *Piezo1* cKO mice. Each mouse received $10^{11}$ GC of both pAAV8-TBG-CCN1 and pAAV8-TBG-CCN2, with a total volume of 30 μL per injection.

### Statistics and reproducibility

Exact sample size for each experiment is provided in the figure legends. Statistical analysis between groups was performed by two-tailed Student's *t* test to determine significance when only two groups were compared. One-way ANOVA with Bonferroni or Holm-Sidak's post-hoc tests was used to compare differences between multiple groups. When two independent variables were tested, two-way ANOVA was performed to determine main effects and interaction effects before comparison of group differences using post-hoc tests. *P*-values for interaction and main effects for all two-way ANOVA tests are reported in Supplementary Table 1. $P < 0.05$ was considered statistically significant. Error bars on all graphs are presented as the SD of the mean unless otherwise indicated. Each data point represents an independent experimental replicate or a biologically independent animal as indicated in the figure legends. All animals are randomly assigned to experimental groups. No data were excluded from the analyses. Investigator performing the quantifications was blinded to the experimental groups to avoid bias. Sample size was determined according to effect size and standard deviations of the most variable parameters based on preliminary experiments with type I error = 0.05 and type II error = 0.2 for a two-sided test.

### Reporting summary

Further information on research design is available in the Nature Portfolio Reporting Summary linked to this article.

## Data availability

Bulk RNA-seq data generated from this study are deposited in NCBI's Gene Expression Omnibus (GEO) with the accession number GSE277264. Reanalysis of a previously published RNA sequencing data set of mouse bones[35] are deposited at ArrayExpress with the accession number E-MTAB-5532. The authors declare that all other data supporting the findings of this study are available within the article and its supplementary materials or from the corresponding author upon reasonable request. Source data are provided with this paper.

## References


1. Mammoto, T. & Ingber, D. E. Mechanical control of tissue and organ development. *Development* **137**, 1407–1420 (2010).
2. Di, X. et al. Cellular mechanotransduction in health and diseases: from molecular mechanism to therapeutic targets. *Signal Transduct. Target Ther.* **8**, 282 (2023).
3. Duncan, R. L. & Turner, C. H. Mechanotransduction and the functional response of bone to mechanical strain. *Calcif. Tissue Int.* **57**, 344–358 (1995).
4. Wang, L., You, X., Zhang, L., Zhang, C. & Zou, W. Mechanical regulation of bone remodeling. *Bone Res.* **10**, 16 (2022).
5. Robling A. G., Turner C. H. Mechanical signaling for bone modeling and remodeling. *Crit. Rev. Eukaryot Gene Expr.* **19**, 319–38 (2009).
6. Stavnichuk, M., Mikolajewicz, N., Corlett, T., Morris, M. & Komarova, S. V. A systematic review and meta-analysis of bone loss in space travelers. *npj Microgravity* **6**, 13 (2020).
7. Schaffler, M. B., Cheung, W.-Y., Majeska, R. & Kennedy, O. Osteocytes: master orchestrators of bone. *Calcif. Tissue Int.* **94**, 5–24 (2014).
8. Wang, Y., McNamara, L. M., Schaffler, M. B. & Weinbaum, S. A model for the role of integrins in flow induced mechanotransduction in osteocytes. *Proc. Natl. Acad. Sci. USA* **104**, 15941–15946 (2007).
9. Qin, L., Liu, W., Cao, H. & Xiao, G. Molecular mechanosensors in osteocytes. *Bone Res.* **8**, 23 (2020).
10. Li, X. et al. Stimulation of Piezo1 by mechanical signals promotes bone anabolism. *Elife* **8**, e49631 (2019).
11. Zhou, T. et al. Piezo1/2 mediate mechanotransduction essential for bone formation through concerted activation of NFAT-YAP1-ss-catenin. Elife. **9**, https://doi.org/10.7554/eLife.52779 (2020).
12. Wang, L. et al. Mechanical sensing protein PIEZO1 regulates bone homeostasis via osteoblast-osteoclast crosstalk. *Nat. Commun.* **11**, 282 (2020).
13. Sun, W. et al. The mechanosensitive Piezo1 channel is required for bone formation. *Elife* **8**, e47454 (2019).
14. Choi, J. U. A., Kijas, A. W., Lauko, J. & Rowan, A. E. The mechanosensory role of osteocytes and implications for bone health and disease states. *Front. Cell Dev. Biol.* **9**, 770143 (2022).
15. Yee, C. S., Schurman, C. A., White, C. R. & Alliston, T. Investigating osteocytic perilacunar/canalicular remodeling. *Curr. Osteoporos. Rep.* **17**, 157–168 (2019).
16. Moharrer, Y. & Boerckel, J. D. Tunnels in the rock: dynamics of osteocyte morphogenesis. *Bone* **153**, 116104 (2021).
17. Wang, J. S. & Wein, M. N. Pathways controlling formation and maintenance of the osteocyte dendrite network. *Curr. Osteoporos. Rep.* **20**, 493–504 (2022).
18. Burra, S. et al. Dendritic processes of osteocytes are mechanotransducers that induce the opening of hemichannels. *Proc. Natl. Acad. Sci.* **107**, 13648–13653 (2010).

19. Wu, D., Schaffler, M. B., Weinbaum, S. & Spray, D. C. Matrix-dependent adhesion mediates network responses to physiological stimulation of the osteocyte cell process. *Proc. Natl. Acad. Sci. USA* **110**, 12096–12101 (2013).
20. Thi, M. M., Suadicani, S. O., Schaffler, M. B., Weinbaum, S. & Spray, D. C. Mechanosensory responses of osteocytes to physiological forces occur along processes and not cell body and require αVβ3 integrin. *Proc. Natl. Acad. Sci.* **110**, 21012–21017 (2013).
21. Doty, S. B. Morphological evidence of gap junctions between bone cells. *Calcif. Tissue Int.* **33**, 509–512 (1981).
22. Milovanovic, P. et al. Br. Osteocytic canalicular networks: morphological implications for altered mechanosensitivity. *ACS Nano* **7**, 7542–7551 (2013).
23. Kobayashi, K. et al. Mitochondrial superoxide in osteocytes perturbs canalicular networks in the setting of age-related osteoporosis. *Sci. Rep.* **5**, 9148 (2015).
24. Tiede-Lewis, L. M. et al. Degeneration of the osteocyte network in the C57BL/6 mouse model of aging. *Aging* **9**, 2190 (2017).
25. Sugawara, Y. et al. The early mouse 3D osteocyte network in the presence and absence of mechanical loading. *Bone* **52**, 189–196 (2013).
26. Karagiosis, S. A. & Karin, N. J. Lysophosphatidic acid induces osteocyte dendrite outgrowth. *Biochem. Biophys. Res. Commun.* **357**, 194–199 (2007).
27. Matsugaki, A., Yamazaki, D. & Nakano, T. Selective patterning of netrin-1 as a novel guiding cue for anisotropic dendrogenesis in osteocytes. *Mater. Sci. Eng. C* **108**, 110391 (2020).
28. Niimura, M. et al. Semaphorin 3A promotes dendrite elongation of osteocytes in association with down-regulation of CDK6. *In Vivo* **30**, 231–236 (2016).
29. Wang, J. S. et al. Control of osteocyte dendrite formation by Sp7 and its target gene osteocrin. *Nat. Commun.* **12**, 6271 (2021).
30. Tang, S. Y., Herber, R. P., Ho, S. P. & Alliston, T. Matrix metalloproteinase–13 is required for osteocytic perilacunar remodeling and maintains bone fracture resistance. *J. Bone Miner. Res.* **27**, 1936–1950 (2012).
31. Dole, N. S. et al. Osteocyte-intrinsic TGF-β signaling regulates bone quality through perilacunar/canalicular remodeling. *Cell Rep.* **21**, 2585–2596 (2017).
32. Kegelman, C. D. et al. YAP and TAZ mediate osteocyte perilacunar/canalicular remodeling. *J. Bone Miner. Res.* **35**, 196–210 (2020).
33. Dupont, S. et al. Role of YAP/TAZ in mechanotransduction. *Nature* **474**, 179–183 (2011).
34. Tanaka-Kamioka, K., Kamioka, H., Ris, H. & Lim, S. S. Osteocyte shape is dependent on actin filaments and osteocyte processes are unique actin-rich projections. *J. Bone Miner. Res.* **13**, 1555–1568 (1998).
35. Youlten, S. E. et al. Osteocyte transcriptome mapping identifies a molecular landscape controlling skeletal homeostasis and susceptibility to skeletal disease. *Nat. Commun.* **12**, 2444 (2021).
36. Bass, S. et al. The differing tempo of growth in bone size, mass, and density in girls is region-specific. *J. Clin. Investig.* **104**, 795–804 (1999).
37. Bradney, M. et al. Heterogeneity in the growth of the axial and appendicular skeleton in boys: implications for the pathogenesis of bone fragility in men. *J. Bone Miner. Res.* **15**, 1871–1878 (2000).
38. Donnelly, E., Boskey, A. L., Baker, S. P. & Van der Meulen, M. C. Effects of tissue age on bone tissue material composition and nanomechanical properties in the rat cortex. *J. Biomed. Mater. Res. A* **92**, 1048–1056 (2010).
39. Debnath, S. et al. Discovery of a periosteal stem cell mediating intramembranous bone formation. *Nature* **562**, 133–139 (2018).
40. Fratzl, P., Gupta, H., Paschalis, E. & Roschger, P. Structure and mechanical quality of the collagen–mineral nano-composite in bone. *J. Mater. Chem.* **14**, 2115–2123 (2004).
41. Vatsa, A. et al. Osteocyte morphology in fibula and calvaria—is there a role for mechanosensing?. *Bone* **43**, 452–458 (2008).
42. Wang, W., Sarazin, B. A., Kornilowicz, G. & Lynch, M. E. Mechanically-loaded breast cancer cells modify osteocyte mechanosensitivity by secreting factors that increase osteocyte dendrite formation and downstream resorption. *Front. Endocrinol.* **9**, 352 (2018).
43. Lu, Y. et al. DMP1-targeted Cre expression in odontoblasts and osteocytes. *J. Dent. Res.* **86**, 320–325 (2007).
44. Cahalan, S. M. et al. Piezo1 links mechanical forces to red blood cell volume. *Elife* **4**, Epub 20150522 (2015).
45. van Tol, A. F. et al. The mechanoresponse of bone is closely related to the osteocyte lacunocanalicular network architecture. *Proc. Natl. Acad. Sci. USA* **117**, 32251–32259 (2020).
46. Kuwahara, S. T. et al. Sox9+ messenger cells orchestrate large-scale skeletal regeneration in the mammalian rib. *Elife* **8**, e40715 (2019).
47. Spatz, J. M. et al. The Wnt inhibitor sclerostin is up-regulated by mechanical unloading in osteocytes in vitro. *J. Biol. Chem.* **290**, 16744–16758 (2015).
48. Syeda, R. et al. Chemical activation of the mechanotransduction channel Piezo1. *Elife.* **4**, https://doi.org/10.7554/eLife.07369 (2015).
49. Totaro, A., Panciera, T. & Piccolo, S. YAP/TAZ upstream signals and downstream responses. *Nat. Cell Biol.* **20**, 888–899 (2018).
50. Ramakrishnan, A. B. & Cadigan, K. M. Wnt target genes and where to find them. *F1000Res.* **6**, 746 (2017).
51. Wang, J. et al. Endothelial Wnts control mammary epithelial patterning via fibroblast signaling. *Cell Rep.* **34**, 108897 (2021).
52. Kastan, N. R. et al. Development of an improved inhibitor of Lats kinases to promote regeneration of mammalian organs. *Proc. Natl. Acad. Sci. USA* **119**, e2206113119 (2022).
53. Liu, J. et al. Targeting Wnt-driven cancer through the inhibition of Porcupine by LGK974. *Proc. Natl. Acad. Sci. USA* **110**, 20224–20229 (2013).
54. Wagner, F. F. et al. Inhibitors of glycogen synthase kinase 3 with exquisite kinome-wide selectivity and their functional effects. *ACS Chem. Biol.* **11**, 1952–1963 (2016).
55. Liu-Chittenden, Y. et al. Genetic and pharmacological disruption of the TEAD-YAP complex suppresses the oncogenic activity of YAP. *Genes Dev.* **26**, 1300–1305 (2012).
56. Li, X. et al. YAP inhibits ERalpha and ER(+) breast cancer growth by disrupting a TEAD-ERalpha signaling axis. *Nat. Commun.* **13**, 3075 (2022).
57. Meyer, K., Lammers, N. C., Bugaj, L. J., Garcia, H. G. & Weiner, O. D. Optogenetic control of YAP reveals a dynamic communication code for stem cell fate and proliferation. *Nat. Commun.* **14**, 6929 (2023).
58. Zanconato, F. et al. Genome-wide association between YAP/TAZ/TEAD and AP-1 at enhancers drives oncogenic growth. *Nat. Cell Biol.* **17**, 1218–1227 (2015).
59. Li, X. et al. Sclerostin binds to LRP5/6 and antagonizes canonical Wnt signaling. *J. Biol. Chem.* **280**, 19883–19887 (2005).
60. van Bezooijen, R. L. et al. Sclerostin is an osteocyte-expressed negative regulator of bone formation, but not a classical BMP antagonist. *J. Exp. Med.* **199**, 805–814 (2004).
61. Yimlamai, D. et al. Hippo pathway activity influences liver cell fate. *Cell* **157**, 1324–1338 (2014).
62. Zhang, L. S. & Lum, L. Delivery of the porcupine inhibitor WNT974 in mice. *Methods Mol. Biol.* **1481**, 111–117 (2016).

63. Diegel, C. R. et al. Inhibiting WNT secretion reduces high bone mass caused by Sost loss-of-function or gain-of-function mutations in Lrp5. *Bone Res.* **11**, 47 (2023).
64. Funck-Brentano, T. et al. Porcupine inhibitors impair trabecular and cortical bone mass and strength in mice. *J. Endocrinol.* **238**, 13–23 (2018).
65. Yadav, V. K. et al. Lrp5 controls bone formation by inhibiting serotonin synthesis in the duodenum. *Cell* **135**, 825–837 (2008).
66. Lau, L. F. Cell surface receptors for CCN proteins. *J. Cell Commun. Signal* **10**, 121–127 (2016).
67. Perbal, B. CCN proteins: a centralized communication network. *J. Cell Commun. Signal* **7**, 169–177 (2013).
68. Nakabayashi, H., Taketa, K., Miyano, K., Yamane, T. & Sato, J. Growth of human hepatoma cell lines with differentiated functions in chemically defined medium. *Cancer Res.* **42**, 3858–3863 (1982).
69. Tang, Q. et al. The membrane-permeable calcium chelator BAPTA-AM directly blocks human ether-a-go-go-related gene potassium channels stably expressed in HEK 293 cells. *Biochem Pharm.* **74**, 1596–1607 (2007).
70. Burra, S., Nicolella, D. P. & Jiang, J. X. Dark horse in osteocyte biology: glycocalyx around the dendrites is critical for osteocyte mechanosensing. *Commun. Integr. Biol.* **4**, 48–50 (2011).
71. Sun, Z., Guo, S. S. & Fassler, R. Integrin-mediated mechanotransduction. *J. Cell Biol.* **215**, 445–456 (2016).
72. Mitra, S. K. & Schlaepfer, D. D. Integrin-regulated FAK-Src signaling in normal and cancer cells. *Curr. Opin. Cell Biol.* **18**, 516–523 (2006).
73. Elbediwy, A. et al. Integrin signalling regulates YAP and TAZ to control skin homeostasis. *Development* **143**, 1674–1687 (2016).
74. Arias-Salgado, E. G. et al. Src kinase activation by direct interaction with the integrin beta cytoplasmic domain. *Proc. Natl. Acad. Sci. USA* **100**, 13298–13302 (2003).
75. Olivares, M. J. et al. Src kinases regulate de novo actin polymerization during exocytosis in neuroendocrine chromaffin cells. *PLoS ONE* **9**, e99001 (2014).
76. Tehrani, S., Tomasevic, N., Weed, S., Sakowicz, R. & Cooper, J. A. Src phosphorylation of cortactin enhances actin assembly. *Proc. Natl. Acad. Sci. USA* **104**, 11933–11938 (2007).
77. Lombardo, L. J. et al. Discovery of N-(2-chloro-6-methyl- phenyl)-2-(6-(4-(2-hydroxyethyl)- piperazin-1-yl)-2-methylpyrimidin-4- ylamino)thiazole-5-carboxamide (BMS-354825), a dual Src/Abl kinase inhibitor with potent antitumor activity in preclinical assays. *J. Med. Chem.* **47**, 6658–6661 (2004).
78. Hsu P. C., Yang C. T., Jablons D. M., You L. The crosstalk between Src and Hippo/YAP signaling pathways in non-small cell lung cancer (NSCLC). Cancers. **12**, https://doi.org/10.3390/cancers12061361. (2020).
79. Lamar, J. M. et al. SRC tyrosine kinase activates the YAP/TAZ axis and thereby drives tumor growth and metastasis. *J. Biol. Chem.* **294**, 2302–2317 (2019).
80. Piccolo, S., Panciera, T., Contessotto, P. & Cordenonsi, M. YAP/TAZ as master regulators in cancer: modulation, function and therapeutic approaches. *Nat. Cancer* **4**, 9–26 (2023).
81. Liu, Y. et al. Yap-Sox9 signaling determines hepatocyte plasticity and lineage-specific hepatocarcinogenesis. *J. Hepatol.* **76**, 652–664 (2022).
82. Bonewald, L. F. The amazing osteocyte. *J. Bone Min. Res.* **26**, 229–238 (2011).
83. Weinbaum, S., Cowin, S. C. & Zeng, Y. A model for the excitation of osteocytes by mechanical loading-induced bone fluid shear stresses. *J. Biomech.* **27**, 339–360 (1994).
84. Han, Y., Cowin, S. C., Schaffler, M. B. & Weinbaum, S. Mechanotransduction and strain amplification in osteocyte cell processes. *Proc. Natl. Acad. Sci.* **101**, 16689–16694 (2004).
85. Steck, R., Niederer, P. & Tate, M. K. A finite element analysis for the prediction of load-induced fluid flow and mechanochemical transduction in bone. *J. Theor. Biol.* **220**, 249–259 (2003).
86. Verbruggen, S. W., Vaughan, T. J. & McNamara, L. M. Mechanisms of osteocyte stimulation in osteoporosis. *J. Mech. Behav. Biomed. Mater.* **62**, 158–168 (2016).
87. Gluhak-Heinrich, J. et al. Mechanical loading stimulates dentin matrix protein 1 (DMP1) expression in osteocytes in vivo. *J. Bone Min. Res.* **18**, 807–817 (2003).
88. Gluhak-Heinrich, J., Pavlin, D., Yang, W., MacDougall, M. & Harris, S. E. MEPE expression in osteocytes during orthodontic tooth movement. *Arch. Oral. Biol.* **52**, 684–690 (2007).
89. Mullen, C. A., Haugh, M. G., Schaffler, M. B., Majeska, R. J. & McNamara, L. M. Osteocyte differentiation is regulated by extracellular matrix stiffness and intercellular separation. *J. Mech. Behav. Biomed. Mater.* **28**, 183–194 (2013).
90. Robling, A. G. et al. Mechanical stimulation of bone in vivo reduces osteocyte expression of Sost/sclerostin. *J. Biol. Chem.* **283**, 5866–5875 (2008).
91. Zhou, Y. et al. Aberrant activation of Wnt signaling pathway altered osteocyte mineralization. *Bone* **127**, 324–333 (2019).
92. Khan, S. K. et al. Induced Gnas(R201H) expression from the endogenous Gnas locus causes fibrous dysplasia by up-regulating Wnt/beta-catenin signaling. *Proc. Natl. Acad. Sci. USA* **115**, E418–E427 (2018).
93. Regard, J. B. et al. Wnt/beta-catenin signaling is differentially regulated by Galpha proteins and contributes to fibrous dysplasia. *Proc. Natl. Acad. Sci. USA* **108**, 20101–20106 (2011).
94. Imajo, M., Miyatake, K., Iimura, A., Miyamoto, A. & Nishida, E. A molecular mechanism that links hippo signalling to the inhibition of Wnt/beta-catenin signalling. *EMBO J.* **31**, 1109–1122 (2012).
95. Cheung, P. et al. Regenerative reprogramming of the intestinal stem cell state via Hippo signaling suppresses metastatic colorectal cancer. *Cell Stem Cell* **27**, 590–604 e9 (2020).
96. Laine, C. M. et al. WNT1 mutations in early-onset osteoporosis and osteogenesis imperfecta. *N. Engl. J. Med.* **368**, 1809–1816 (2013).
97. McBride S. H., Silva M. J. Adaptive and injury response of bone to mechanical loading. *Bonekey Rep.* **1**, https://doi.org/10.1038/bonekey.2012.192 (2012).
98. Jiang, L., Li, J., Zhang, C., Shang, Y. & Lin, J. YAP-mediated crosstalk between the Wnt and Hippo signaling pathways (Review). *Mol. Med. Rep.* **22**, 4101–4106 (2020).
99. Rausch, V. & Hansen, C. G. The hippo pathway, YAP/TAZ, and the plasma membrane. *Trends Cell Biol.* **30**, 32–48 (2020).
100. Kawaki, H. et al. Differential roles of CCN family proteins during osteoblast differentiation: involvement of Smad and MAPK signaling pathways. *Bone* **49**, 975–989 (2011).
101. Chen, L. & Brigstock, D. R. Analysis of pathological activities of CCN proteins in fibrotic diseases: liver fibrosis. *Methods Mol. Biol.* **1489**, 445–463 (2017).
102. Ju, L. et al. CCN1 promotes hepatic steatosis and inflammation in non-alcoholic steatohepatitis. *Sci. Rep.* **10**, 3201 (2020).
103. Yu, Y. E., Hu, Y. J., Zhou, B., Wang, J. & Guo, X. E. Microstructure determines apparent-level mechanics despite tissue-level anisotropy and heterogeneity of individual plates and rods in normal human trabecular bone. *J. Bone Miner. Res.* **36**, 1796–1807 (2020).
104. Hu, Y. J. et al. Mechanical and structural properties of articular cartilage and subchondral bone in human osteoarthritic knees. *J. Bone Miner. Res.* **39**, 1120–1131 (2024).
105. Oliver, W. C. & Pharr, G. M. An improved technique for determining hardness and elastic modulus using load and displacement sensing indentation experiments. *J. Mater. Res.* **7**, 1564–1583 (1992).
106. Robinson, M. D. & Oshlack, A. A scaling normalization method for differential expression analysis of RNA-seq data. *Genome Biol.* **11**, R25 (2010).

107. Yu, G., Wang, L. G., Han, Y. & He, Q. Y. clusterProfiler: an R package for comparing biological themes among gene clusters. *OMICS* **16**, 284–287 (2012).

## Acknowledgements

The studies conducted are supported by the Department of Defense (W81XWH2110449, Y.Y.), National Institutes of Health (R01DE025866, Y.Y.), and the Forsyth Postdoctoral Training grant in Oral Health Research (5T90DE026110, Y.J.H.). We thank the Yang lab members for the stimulating discussions. We are grateful to Dr. X. Edward Guo for providing samples of the *Sost* KO mice and access to the microindentation testing system. We acknowledge the Microscopy Resources on the North Quad (MicRoN) core at Harvard Medical School for providing training and equipment for image acquisition.

## Author contributions

Conceptualization: Y.Y., Y.J.H., X.W. Methodology: Y.J.H., X.W., Y.J. (Yu Jin), Y.L. Investigation: J.Y.H., X.W., F.W., Y.J. (Yu Jin), Y.J. (Yangchen Jin), Y.L., Q.C. Visualization: J.Y.H., Y.J. (Yu Jin). Funding acquisition: Y.Y., Y.J.H. Project administration: Y.Y. Supervision: Y.Y. Writing—original draft: Y.J.H., Y.Y. Writing – review & editing: Y.J.H., Y.Y.

## Competing interests

The authors declare no competing interests.

## Additional information

**Supplementary information** The online version contains supplementary material available at https://doi.org/10.1038/s41467-025-65636-9.

**Correspondence** and requests for materials should be addressed to Yingzi Yang.

**Peer review information** *Nature Communications* thanks the anonymous reviewers for their contribution to the peer review of this work. A peer review file is available.